Regulation of neural stem cell differentiation and brain development by MGAT5-mediated N-glycosylation

Andrew R. Yale^{1,2,3}, Estelle Kim^{2,3}, Brenda Gutierrez^{1,2,3}, J. Nicole Hanamoto^{2,3}, Nicole S. Lav³, Jamison L. Nourse^{2,3}, Marc Salvatus³, Robert F. Hunt^{1,3}, Edwin S. Monuki^{3,4}, Lisa A. Flanagan*^{1,2,3,5}

¹Department of Anatomy & Neurobiology, University of California Irvine, Irvine, CA 92697, USA

²Department of Neurology, University of California Irvine, Irvine, CA 92697, USA

³Sue & Bill Gross Stem Cell Research Center, University of California Irvine, Irvine, CA 92697, USA

⁴Department of Pathology and Laboratory Medicine, University of California Irvine, Irvine, CA 92697, USA

⁵Department of Biomedical Engineering, University of California Irvine, Irvine, CA 92697, USA

*Correspondence: <u>lisa.flanagan@uci.edu</u>

Summary

Undifferentiated neural stem and progenitor cells (NSPCs) encounter extracellular signals that bind plasma membrane proteins and impact differentiation. Membrane proteins are regulated by N-linked glycosylation, making it possible that glycosylation plays a critical role in cell differentiation. We assessed enzymes that control N-glycosylation in NSPCs and found loss of the enzyme responsible for generating β1,6 branched N-glycans, N-acetylglucosaminyltransferase V (MGAT5), led to specific changes in NSPC differentiation *in vitro* and *in vivo*. *Mgat5* homozygous null NSPCs in culture formed more neurons and fewer astrocytes compared to wild-type controls. In the brain cerebral cortex, loss of MGAT5 caused accelerated neuronal differentiation. Rapid neuronal differentiation led to depletion of cells in the NSPC niche, resulting in a shift in cortical neuron layers in *Mgat5* null mice. Glycosylation enzyme MGAT5 plays a critical and previously unrecognized role in cell differentiation and early brain development.

Keywords: neural stem cell; neuron; astrocyte; brain; cerebral cortex; N-glycan branching

Introduction

In the central nervous system (CNS), neural stem and progenitor cells (NSPCs) differentiate into neurons at early stages and later form glia (astrocytes and oligodendrocytes) to construct the brain and spinal cord. Neural stem cells in the cerebral cortex of the developing brain occupy a niche next to the lateral ventricle termed the ventricular zone. During neurogenesis, neural stem cells produce progenitors that form newborn neurons that migrate away from the ventricular surface to construct the cortical plate. The earliest born neurons create the deep layers of the cortical plate and later born neurons migrate past the deep layers to make superficial neuronal layers near the pial surface. This wave of neurogenesis is followed by the formation of astrocytes. Cortical NSPCs can differentiate into oligodendrocytes, but most oligodendrocytes derive from the ganglionic eminence and migrate into the cortex (He et al. 2001). Identifying the cellular processes controlling NSPC differentiation into neurons and astrocytes is critical for understanding cortical development.

Undifferentiated stem cells encounter myriad extracellular signals, such as cell adhesion molecules, growth factors and morphogens, that impact differentiation through binding to plasma membrane proteins (Taverna et al. 2014). Glycosylation is a major plasma membrane protein post-translational modification in which sugar molecules, known as glycans, are attached to asparagine (N-linked) or serine/threonine (O-linked) amino acids (Ohtsubo and Marth 2006). Most cell surface protein extracellular domains are N-link glycosylated, and the presence and type of glycans can regulate protein function, localization at the cell surface and ligand affinity (Ohtsubo and Marth 2006).

Distinct patterns of plasma membrane N-glycans distinguish neuron- and astrocyte-biased NSPCs (Yale et al. 2018). Specifically, the N-glycan branching pathway that generates complex, highly branched sugars on plasma membrane proteins differs in these cells; branching is low on neuron-biased NSPCs and high on astrocyte-biased cells (Yale et al. 2018). Expression of branched N-glycans on NSPCs in the ventricular zone/subventricular zone (VZ/SVZ) of the developing embryonic cortex *in vivo* is low at early, neurogenic stages but high during later astrogenesis (Yale et al. 2018). Pharmacologically enhancing N-glycan branching on cultured NSPCs reduces neuron formation and stimulates differentiation into astrocytes without affecting cell viability or proliferation (Yale et al. 2018). Glycosylation thus regulates neural differentiation, and it will be important to identify enzymes in the branching pathway that impact NSPC differentiation and test whether they regulate NSPC function *in vitro* and *in vivo*.

N-glycan branching is controlled by sequentially acting enzymes in the endoplasmic reticulum and Golgi apparatus. Particularly important are the mannosidase enzymes that remove mannose, freeing sites for attachment of N-acetylglucosamine (GlcNAc) residues, and the N-acetylglucosaminyltransferases (MGATs) that add GlcNAc to available sites to create N-glycan branches. MGAT activity is essential for proper CNS development since reducing the expression of enzymes that generate branched N-glycans results in severe developmental abnormalities (Schachter 2001). For example, deficiency of MGAT1 causes failure in neural tube closure and is embryonic lethal (loffe and Stanley 1994, Metzler et al. 1994). Patients with mutations in the *MGAT2* gene (congenital disorder CDG IIa) and mice with *Mgat2* deletions exhibit CNS symptoms, including psychomotor retardation and cognitive deficits, and die prematurely (Schachter 2001, Wang et al. 2002).

Despite the importance of glycosylation in CNS development, no links between specific glycosylation enzymes and NSPC differentiation have been described. Here, we use pharmacologic agents and knockout mice to determine whether enzymes of the N-glycan branching pathway impact NSPCs and serve as critical regulators of cell differentiation.

Results

Increasing N-glycan branching alters NSPC fate but blocking early branching enzymes does not

We found previously that treating undifferentiated NSPCs with the substrate GlcNAc to stimulate N-glycan branching reduced neurogenesis and enhanced astrogenesis (Yale et al. 2018). We hypothesized that decreasing branched N-glycans would have the opposite effect and tested this by blocking enzymes early in the branching pathway. We used Kifunensine (Kif) to inhibit alpha-mannosidase 1 (MAN1) (Males et al. 2017), which cleaves excess mannose residues to enable addition of GlcNAc to initiate N-glycan branching (Figure 1A). We treated mouse embryonic day 12.5 (E12) cortical NSPCs with a Kif dose range, used L-PHA lectin to detect branched N-glycans, and determined that 0.5 μ M Kif resulted in an almost complete reduction in L-PHA binding (Figure S1A, B).

E12 NSPCs were treated with GlcNAc to increase or Kif to reduce N-glycan branching and lectin flow cytometry was used to compare cell surface N-glycans. GlcNAc-treated NSPCs had significantly increased β 1,4 (MGAT4 product) and β 1,6 (MGAT5 product) branched N-glycans detected by lectins DSL and L-PHA (Figure 1A-C). NSPCs treated with Kif had reduced levels of bisecting branches (E-PHA), β 1,4 branches (DSL), β 1,6 branches (L-PHA) and core fucose (LCA) and increased levels of high mannose (ConA) and LEA binding (Figure 1D). LEA detects N-acetyllactosamine but also binds high mannose structures, which LEA is likely detecting on Kif treated cells since they have increased ConA binding and reduced β 1,4 and β 1,6 branches from which N-acetyllactosamine extends (Oguri 2005). Hence, Kif treatment induced widespread changes to cell surface N-glycans that included, but were not limited to, branched N-glycans.

We tested whether N-glycan branching affected differentiation by treating undifferentiated E12 NSPCs with GlcNAc or Kif, differentiating the cells, and measuring the formation of neurons and astrocytes. As we found previously, NSPCs treated with GlcNAc differentiated into significantly fewer neurons and more astrocytes compared to untreated controls (Figures 1E, S1C) (Yale et al. 2018). In contrast, differentiation was not affected by Kif treatment (Figure 1E). NSPCs from later developmental stages (E16 and E18) express higher levels of branched N-glycans, so might be more affected by Kif (Yale et al. 2018). However, Kif treatment of E16 and E18 NSPCs did not significantly impact differentiation (Figure S1D, E). We also tested whether other agents that affect early enzymes in the branching pathway or treatment of NSPCs throughout differentiation would have an impact. We used deoxymannojirimycin (DMJ) to inhibit MAN1 or swainsonine (SW) to block MAN2 and treated E12 and E16 NSPCs for 3 days as undifferentiated cells and during 3 days of differentiation (Figure S1F). There was no significant difference in the differentiation of E12 or E16 NSPCs treated with DMJ or SW (Figure S1G). These data agree with the Kif data (Figure 1E, Figure S1D, E) and confirm that blocking early enzymes in the N-glycan branching pathway does not alter NSPC differentiation. Thus, NSPC neuronal and astrocytic differentiation is altered by GlcNAc treatment that enhances branching but not by disruption of MAN1 or MAN2.

MGAT5 knockout blocks the production of β1,6 branched N-glycans and alters NSPC fate in vitro

Since blocking mannosidase enzymes early in the N-glycan branching pathway did not alter differentiation, we hypothesized that later enzymes might be critical. We assessed N-glycosylation enzyme expression in mouse NSPCs by RNAseq and identified those affecting mannose, branching, fucose, sialic acid, and polylactosamine (Figure S2) (Yale et al. 2018).

Since GlcNAc treatment alters NSPC fate, we focused on MGATs that add GlcNAc to create branches (Figure 1A, E). NSPCs express MGAT5, which adds a β 1,6 GlcNAc to the trimannosyl core to produce branched N-glycans detected by L-PHA (Figures 1A, 2A). L-PHA binding is increased after GlcNAc treatment that affects NSPC differentiation (Figure 1C, E) and is higher at astrogenic compared to neurogenic stages of cortical development (Yale et al. 2018). Additionally, astrocyte-biased NSPCs express higher levels of MGAT5 compared to neurogenic NSPCs (Yale et al. 2018). We therefore wondered whether disruption of MGAT5 would decrease β 1,6 branching and alter differentiation.

We analyzed E12 NSPCs isolated from Mgat5 wild type (WT), heterozygous, and null animals (Granovsky et al. 2000). Comparison of WT and null NSPC glycosylation enzyme transcripts by qRT-PCR revealed the expected Mgat5 loss but no change in other enzymes (Figure 2B). Lectin flow cytometry showed that L-PHA binding (β 1,6 branched N-glycans) was significantly reduced on Mgat5 heterozygous and virtually abolished on null NSPCs (Figure 2C). While null NSPCs did not have lower expression of the Mgat4a and 4b enzymes that generate the β 1,4 branch, they showed reduced DSL binding (Figure 2B, C). This could be due to the fact that DSL has higher affinity for β 1,4 branched glycans that also contain a β 1,6 branch (Abbott and Pierce 2010, Hirabayashi et al. 2015).

We assessed differentiation and found *Mgat5* heterozygous and null E12 NSPCs formed significantly more neurons compared to WT cells (Figure 2D), while *Mgat5* null NSPCs generated significantly fewer astrocytes (Figure 2E). Although E12 cortical NSPCs generate relatively few oligodendrocytes, we measured oligodendrocyte differentiation and found no difference among *Mgat5* WT, heterozygous and null NSPCs (Figure S2B). These experiments demonstrate that MGAT5 loss enhances neuron differentiation and reduces astrocyte formation *in vitro*. Increasing branching with GlcNAc treatment (Figure 1) and decreasing branching with targeted disruption of MGAT5 (Figure 2) produce opposite effects on NSPC differentiation, showing that N-glycan branching regulates NSPC differentiation and fate.

Altered NSPC proliferation or viability could impact differentiation, so we tested whether *Mgat5* WT and mutant NSPCs differed in these parameters. NSPC proliferation was analyzed by multiple assays. Ki67 detects cycling cells and we found no difference among *Mgat5* WT and mutant NSPCs (Figure 2F). EdU incorporation measures cells in S-phase and there was a significant increase in *Mgat5* null compared to WT or heterozygous NSPCs (Figure 2F). Phosphorylated histone H3 labels cells in M-phase and there was no difference among *Mgat5* WT, heterozygous and null cells (Figure 2F). Thus, the only difference between WT and mutant cells was in EdU incorporation, which reflects new DNA synthesis. Since DNA synthesis can occur independently of cell division, as happens during gene duplication, repair, or apoptosis (Breunig et al. 2007), we used an additional assay to detect dividing cells. Flow cytometry with propidium iodide labeling of nuclear content to measure all cell cycle stages in the same population of cells showed no significant differences in the percentages of cells in G₀/G₁, S, or G₂/M phases across genotype (Figure 2G). Cell viability did not differ for *Mgat5* wT and mutant NSPCs (Figure 2H). Taken together, these data suggest that WT and *Mgat5* null NSPCs are similar in proliferative ability and viability.

MGAT5 loss in vivo increases neuronal differentiation

We assessed the role of MGAT5 in cell differentiation during development by analyzing WT and mutant brains. We measured L-PHA binding to E16 mouse brain sections and found β1,6 branched N-glycans were somewhat reduced in the *Mgat5* heterozygous brain and absent in the null brain (Figure S3A). These data, coupled with the flow cytometry analysis of WT and

Mgat5 mutant NSPCs (Figure 2C), confirm that loss of MGAT5 significantly decreases β1,6 branched N-glycans in the brain.

We assessed NSPC differentiation *in vivo* by staining E16 brain sections with antibodies for neurons: class III β tubulin (TuJ1 antibody, detects neuronal processes) or RBFOX3 (NeuN antibody, detects fully differentiated neuron nuclei). There was a notable increase in TuJ1 and NeuN staining in the E16 *Mgat5* null cortex compared to WT (Figure 3A, B). We found a significant increase in the percentage of NeuN-positive cells in *Mgat5* null cortical plate (CP) at 3 spatially distinct regions of the cortex: medial (toward the midline), dorsal (at the apex of the cortex), and lateral (near the junction with the ganglionic eminence) (Figure 3C). Similarly, there was a significant increase in the number of NeuN-positive cells per mm² in the dorsal CP (Figure 3C). These data show that *Mgat5* null mice have a higher proportion of fully differentiated NeuN-positive neurons compared to WT at E16.

We tested whether *Mgat5* null mice have defects in the localization of differentiated neurons by analyzing NeuN in the intermediate zone (IZ), which contains newly born and migrating neurons, and the VZ/SVZ, which is the NSPC niche. Very few NeuN-positive cells were detected in the E16 IZ and VZ/SVZ and there was no difference across genotype (Figure S3B-D), indicating that MGAT5 depletion did not alter the spatial distribution of differentiated neurons or their migration to the CP.

Since neurogenesis is still underway at E16, we analyzed WT and *Mgat5* null brains at postnatal day 7 (P7) when neurogenesis is complete. By P7, the increase in fully differentiated neurons in *Mgat5* null compared to WT was dampened (Figure 3D, E). These data suggest that neuronal differentiation in WT animals caught up to that of *Mgat5* nulls by postnatal stages.

Enhancing branched N-glycans on NSPCs with GlcNAc treatment increased generation of GFAP-positive astrocytes, and NSPCs lacking MGAT5 form fewer astrocytes *in vitro* (Figures 1E, 2E)(Yale et al. 2018). We therefore assessed GFAP-positive astrocytes in *Mgat5* WT and null brains. In the brain, GFAP expression is high in fibrous astrocytes (Rowitch and Kriegstein 2010). GFAP-positive astrocytes were not detected in E16 or P1 brains (data not shown). By P7, GFAP-positive astrocytes were apparent and primarily restricted to regions near the pial surface of the medial cingulate cortex and the white matter tracts of the external capsule, cingulum, and corpus callosum (Figure S4A, B). We quantified GFAP labeling and found a slight, but not statistically significant, reduction in GFAP staining in the *Mgat5* null brain (Figure S4C). A caveat for comparing the GFAP *in vitro* and *in vivo* findings is that GFAP is not a nuclear marker, making it difficult to determine the percentage of GFAP-positive cells *in vivo*.

We assessed cell proliferation and death in *Mgat5* WT and null brains since these could affect neuronal differentiation *in vivo*. We found no difference in Ki67-positive cycling cells in the E16 WT and *Mgat5* null VZ/SVZ (Figure 3F, S4D). Neuronal number in the cortex is impacted by both generation of neurons and later pruning mechanisms in which unnecessary neurons undergo apoptosis. We stained for cleaved Caspase-3, a marker of apoptotic cells, and found no staining at E16 in WT or *Mgat5* null brains (data not shown). At P7, there was no difference in the number of cells labeled with cleaved Caspase-3 between WT and null brains (Figure 3G, S4E) and the distribution of labeled cells across the neocortex was similar across genotype. Our data indicate that cell proliferation and viability are not substantially altered in the absence of MGAT5 (Figures 2, 3).

Decreased cell numbers and thickness of Mgat5 null brains

The increase in NeuN-positive differentiated neurons in *Mgat5* null animals could cause an overall increase in cell number or CP thickness if excess neurons are generated. However,

analysis of the E16 CP showed that loss of MGAT5 caused significant decreases in cell density (cells/mm²) in medial and lateral CP, the thickness of dorsal and lateral CP, and the total number of cells in medial, dorsal, and lateral CP (Figure 4A). The entire E16 cortex, which includes the CP, IZ, and VZ/SVZ, showed significant decreases in cell density in lateral cortex, thickness of dorsal and lateral cortex, and total number of cells in dorsal and lateral cortex in *Mgat5* null animals compared to WT (Figure 4A). Overall, these data show that the E16 *Mgat5* null brain has significantly decreased numbers of cells and thickness compared to the WT brain.

We analyzed P7 WT and *Mgat5* null neocortex to determine whether MGAT5 loss impacted the total number of cells or cortical architecture at postnatal stages. The cell density in upper layers 2/3 and deep layers 5/6 was significantly lower in *Mgat5* null compared to WT (Figure 4B). We analyzed the neocortex from the pial surface to the top of the corpus callosum and found significantly reduced thickness in *Mgat5* null brains (Figure 4C). Layer analysis revealed that layer 2/3 thickness did not differ between WT and null but there was a significant decrease in the thickness of layers 4 and 5/6 in the *Mgat5* null brain compared to WT (Figure 4C).

Mgat5 null animals have an increase in NeuN-positive fully differentiated neurons but a decrease in cell number, suggesting that the NeuN findings are not due to an increase in neuron number. Further, we did not observe shifts in cell proliferation, migration or death that could account for the lower cell numbers in Mgat5 nulls. These data raise the possibility that MGAT5 loss could lead to an acceleration of neuronal differentiation, causing depletion of progenitors and subsequent reduction in the total number of cells. We therefore analyzed progenitors in the VZ/SVZ at E16.

MGAT5 deficiency depletes a subset of neural progenitors in the embryonic VZ/SVZ

To assess progenitors, we focused on the VZ/SVZ stem and progenitor cell niche. There was a significant decrease in both cell density and total cell number in the *Mgat5* null dorsal and lateral E16 VZ/SVZ compared to WT but no change in thickness (Figure 5A). These data indicate reduced numbers of stem and progenitor cells in *Mgat5* nulls that is not due to an overt change in the number of proliferating or viable cells (Figures 2, 3). We stained the VZ/SVZ with BRN2, which is expressed by upper layer neuron progenitors at E16 and is critical for instructing upper layer neuron identity (Sugitani et al. 2002, Dominguez et al. 2013). There was a significant decrease in the percentage and total number of BRN2-positive progenitors in the VZ/SVZ of *Mgat5* null mice compared to WT (Figure 5B, S5A). We analyzed SOX2, a general progenitor marker, and TBR2, a neuron progenitor marker. SOX2 primarily labeled cells along the ventricle and showed no significant difference between WT and *Mgat5* nulls (Figure S5B). There was no difference in TBR2-positive cells between WT and *Mgat5* null brains (Figure S5C). These data indicate that some, but not all, progenitors are decreased in the *Mgat5* null VZ/SVZ, suggesting a partial depletion of the progenitor pool that could lead to a reduction in neuron numbers in the cortex.

The E16 IZ contains cells migrating from the VZ/SVZ to the CP. We assessed cell number and thickness of the E16 IZ and found *Mgat5* null animals had significant decreases in the number of cells in lateral regions and decreased IZ thickness in dorsal and lateral regions (Figure S5D). In contrast, there was an increase in cells/mm² in the *Mgat5* null medial region (Figure S5D). Since there was a decrease in VZ/SVZ and IZ cells and fewer upper layer neuron progenitors in *Mgat5* nulls at E16, we analyzed cortical layer formation.

Progenitor depletion in mice lacking MGAT5 alters neuronal layers

The cortex is composed of 6 layers and deep layer neurons form first and upper layers follow during development. We stained E16 brains with TBR1 (for earlier born deep layer 6 neurons), CTIP2 (deep layers 5/6), and BRN2 (upper layers 2/3). Since the medial region includes the

newly developing hippocampus, we focused analyses on dorsal and lateral cortical regions. There was a significant decrease in TBR1-positive deep layer neurons in the *Mgat5* null lateral CP and cortex at E16 (Figure 6A, S6A). CTIP2-positive deep layer neurons showed a slight but not significant decrease in the null dorsal CP and cortex and no difference between WT and nulls in the lateral CP and cortex at E16 (Figure S6B). There was a modest and not significant decrease in the number of BRN2-positive upper layer neurons in the *Mgat5* null dorsal CP compared to WT at E16 (Figure S6C). These data suggest that at E16, when cortical layers are still developing, the only detectable difference between WT and null is the earlier born deep layer 6 neurons.

We analyzed cortical layers at P7, when neurogenesis is complete and all layers are fully formed. *Mgat5* null animals have a significant reduction in the number of BRN2-positive upper layer neurons at P7 (Figure 6B, C). These data are consistent with the observed decrease in BRN2-positive progenitors in the VZ/SVZ at E16 in *Mgat5* nulls compared to WT (Figure 5B). There was a significant decrease in CTIP2-positive deep layer neurons in *Mgat5* null animals compared to WT at P7 (Figure 6B, D). Progenitor depletion would be expected to affect upper layers more profoundly than deep since fewer progenitors would be present at later developmental stages when upper layers are formed. We generated a ratio of the number of upper to deep layer neurons (BRN2:CTIP2) for WT and *Mgat5* null brains and found a significant decrease in the ratio in null animals compared to WT, suggesting that later born upper layer neurons were disproportionately affected during *Mgat5* null brain development (Figure 6E). Collectively, our data are consistent with accelerated neuronal differentiation and depletion of progenitors in the *Mgat5* null brain, leading to fewer cells in the cortex and a greater impact on later born upper layer neurons since the effect of progenitor depletion is more profound at later stages.

Discussion

Glycosylation, cell differentiation, and brain development

Extracellular cues impact differentiation, but how cells regulate the plasma membrane to modulate responses to these cues is not well understood. N-glycan branching affects cell surface residence time, ligand affinity and function of many plasma membrane proteins, directly transforming the ability of receptors to bind extracellular cues and stimulate intracellular cascades. Cell surface proteins regulated by N-glycan branching include cell adhesion molecules, growth factor receptors, and ion channels that could affect cell differentiation (Zhao et al. 2008, Dennis et al. 2009, Scott and Panin 2014). Our data now show that cells can alter the plasma membrane glycome via the enzyme MGAT5 to impact cell differentiation. MGAT5 affects NSPC differentiation in several key ways. Loss of MGAT5 decreases β1,6 branched N-glycans and accelerates neuronal differentiation *in vitro* and *in vivo*, leading to a depletion of progenitors *in vivo* that alters layer formation (Figure 7).

Mgat5 null NSPCs in vitro lack β1,6 branches and form more neurons compared to WT cells. This is consistent with our finding that increasing β1,6 branches on NSPCs in vitro with GlcNAc treatment decreases neuronal differentiation (Yale et al. 2018). In vivo, rapid neuron generation leads to more fully differentiated neurons in the Mgat5 null E16 CP compared to WT. Our data do not suggest that MGAT5 alters neuronal migration since there is no increase in NeuN positive neurons in the E16 VZ/SVZ or IZ of Mgat5 null animals, which would be expected if neurons were stuck in those regions instead of migrating properly to the CP.

Rapid neuronal differentiation decreases progenitors in the *Mgat5* null NSPC niche, shown by cell reduction in the VZ/SVZ and fewer BRN2-positive upper layer neuron progenitors at E16 in

Mgat5 nulls compared to WT. Since there was no clear difference in proliferation between WT and *Mgat5* null cells *in vitro* and *in vivo*, reduced cells in the *Mgat5* null VZ/SVZ is not caused by a proliferation defect. Cell death is also not a likely cause since there was no difference in either the live cell percentage between *Mgat5* null and WT NSPCs *in vitro* or the cleaved Caspase-3 apoptotic cells *in vivo* between null and WT. Coupled with the NeuN data, the reduced numbers of progenitors is likely due to their rapid progression from progenitor cells to fully differentiated neurons in *Mgat5* null brains.

As progenitors decrease during *Mgat5* null brain development, there are fewer left to generate neurons. This can be seen with analysis of layer specific markers at different developmental stages. At 16, early born TBR1-positive deep layer neurons are decreased in *Mgat5* nulls, but it is too early to see a clear effect on upper layer neurons. By P7, both deep and upper layers are reduced in *Mgat5* nulls, but the effect is more profound for the later born upper layer neurons. This is consistent with the observed reduction in BRN2-positive upper layer neuron progenitors in the *Mgat5* null VZ-SVZ at E16 and indicates gradual progenitor depletion over time that leaves fewer progenitors at later stages to form upper layer neurons.

The data lead to a model in which MGAT5 activity during normal cortical development increases cell surface β 1,6 branched N-glycans that in turn prevent precocious neuronal differentiation. These findings identify a new role for glycosylation in neural development and show the enzyme MGAT5 and the production of β 1,6 branched N-glycans are critical determinants of cell differentiation.

Rapid neuronal differentiation in MGAT5 deficient mice could impact brain function. Mgat5 null mice appear grossly normal, but exhibit behavioral abnormalities including failure to nurture pups and decreased depressive-like behaviors (Granovsky et al. 2000, Soleimani et al. 2008, Feldcamp et al. 2016). A human genome-wide association study found a link between symptoms of depression and a site in the genome near *Mgat5* (Luciano et al. 2012). Early, subtle or transient abnormalities during brain development can have long lasting impacts on adult behavior. For example, mutations in disheveled, which is important in the Wnt/β-catenin pathway, cause abnormal expansion of deep layer neurons due to rampant neuron progenitor expansion and early neuronal differentiation (Belinson et al. 2016). The effects are transient, however, and the adult brain appears normal. Despite normal brain morphology, adult mutant mice display a number of behavioral deficits including abnormal social interactions and repetitive behaviors (Belinson et al. 2016). Transient pharmacological activation of the Wnt pathway during embryonic stages revived signaling, reversed the developmental abnormality in neuron production, and corrected the adult behavioral phenotype (Belinson et al. 2016). Thus, events occurring early in development can have profound effects on later brain function, even if the adult brain morphology is grossly normal.

A concern for any transgenic or knockout mouse experiment is whether genetic background influences the phenotype. For example, gene loss may be lethal in an inbred mouse strain but not in an outbred strain. Ideally, phenotype would be assessed across multiple strains in any knockout mouse experiment, but this is not always feasible. We suspect our Mgat5 null mice findings are not purely strain dependent since we see consistent effects of branched N-glycans on NSPC fate across mouse strains and in multiple species. Loss of β 1,6 branched N-glycans in C57BL/6 Mgat5 nulls increased neuron differentiation (Figures 2, 3) whereas GlcNAc treatment to increase β 1,6 branched N-glycans on CD1 mouse NSPCs (Figure 1 and (Yale et al. 2018)) and human NSPCs (our unpublished data) had the opposite effect. Thus, the effects of β 1,6 branched N-glycans on cell differentiation are not limited to a single mouse strain.

Regulation of glycosylation and cell differentiation

We identify here the importance of MGAT5 in NSPC differentiation, but an outstanding question is whether other enzymes such as MGAT3 and MGAT4 also play a role. Mouse NSPCs express MGAT3, which adds a bisecting GlcNAc that prevents further branching by MGAT5; MGAT3 thus antagonizes MGAT5 function and high MGAT3 activity would reduce β1,6 branches and mimic loss of MGAT5 (Brockhausen et al. 1988, Zhao et al. 2006). We previously reported that astrocyte-biased NSPCs expressed higher levels of Mgat5 RNA, whereas neuron-biased NSPCs express more Mgat3 (Yale et al. 2018). Neurons differentiated from pluripotent stem cells upregulate MGAT3 and have high cell surface bisecting N-glycans compared to differentiated astrocytes (Terashima et al. 2014). The balance of MGAT5 and MGAT3 activity regulates several cell surface proteins impacting cell function, particularly integrins and cadherins (Zhao et al. 2006, Pinho et al. 2009). Mouse NSPCs express Mgat4a and Mgat4b but little to no Mgat4c. MGAT4 adds a β1,4 branch (detected by DSL) to contribute to N-glycan branching. The loss of Mgat5 did not affect expression of Mgat4a and Mgat4b, but DSL binding was increased on NSPCs after GlcNAc treatment and decreased on Mgat5 null NSPCs (Figures 1, 2). This could be due to several factors, including the higher affinity of DSL for glycans containing both β1,4 and β1,6 branches (Abbott and Pierce 2010, Hirabayashi et al. 2015). MGAT4 expression did not prevent the functional consequences of MGAT5 loss in NPSCs, but analysis of cells and tissue lacking MGAT4 will be important for determining the importance of the \$1.4 branch in cell differentiation and neural development. Of note, MGAT3 activity also blocks further branching by MGAT4 (Brockhausen et al. 1988). Future studies of MGAT3, MGAT4 and MGAT5 will investigate their interconnected roles in NSPC differentiation and map which N-glycans are altered on cells that differ in fate.

Glycosylation could affect differentiation of many cell types. An electrophysiological measure, whole cell membrane capacitance, reflects cell surface glycosylation and distinguishes NSPCs on the basis of neuron or astrocyte fate bias (Labeed et al. 2011, Nourse et al. 2014, Yale et al. 2018, Adams et al. 2020). Treatment of NSPCs with GlcNAc increases membrane capacitance and shifts differentiation (Yale et al. 2018). Membrane capacitance is also linked to differentiation in the mesenchymal/adipose-derived, hematopoietic, and embryonic stem cell lineages (Lee et al. 2018). Mesenchymal stem cell differentiation to adipose vs osteogenic lineages is accompanied by differences in both membrane capacitance (Hildebrandt et al. 2010, Bagnaninchi and Drummond 2011) and glycosylation (Heiskanen et al. 2009, Hamouda et al. 2013). Ties between glycosylation, membrane capacitance, and cell differentiation are evident in multiple stem cell lineages and should be explored further.

Experimental Procedures

Resource availability

Corresponding author

Further information and requests for resources and reagents should be directed to and will be fulfilled by the corresponding author, Lisa Flanagan (lisa.flanagan@uci.edu).

Materials availability

This study did not generate new unique reagents.

Data and code availability

Data will be shared with the research community upon request to the authors. No code or standardized datasets were generated.

Animals

All animal procedures were in accordance with protocols approved by the University of California, Irvine Institutional Animal Care and Use Committee and adhered to National

Institutes of Health Guidelines for the Care and Use of Laboratory Animals. Mice were CD1 (Charles River) or *Mgat5* C57BL/6 nulls (Lee et al. 2007). Genotyping was as described in Supplemental Information.

Cell culture, treatment, and analysis

NSPCs were isolated from E12 mouse dorsal forebrain cortical tissue and grown in culture and differentiated as described in (Yale et al. 2018) and Supplemental Information. For CD1 mice, tissue from multiple embryos in the same litter was pooled, and the culture from a single litter was considered a biological repeat. For *Mgat5* mice, tissue from each embryo was kept separate for genotyping and culture and considered a biological repeat. Comparisons across genotype utilized at least 3 embryos per genotype from separate litters (not littermates). NSPCs were treated with 80 mM GlcNAc and 0.5 µM Kif as described in (Yale et al. 2018) and Supplemental Information. Live E12 NSPCs were dissociated for flow cytometry and RNA isolation or fixed, immunostained, and quantified as described in (Yale et al. 2018) and Supplemental Information (Tables S1 for qRT-PCR primers and S2 for antibodies and lectins). RNAseq data was from E12 CD1 mouse NSPCs from three separate litters as described in Supplemental.

Preparation, staining and analysis of brain sections

Whole brains were dissected from *Mgat5* mice, fixed in paraformaldehyde, frozen, and 12 µm coronal sections prepared as described in Supplemental Information. Brain sections were stained as described in (Yale et al. 2018) and Supplemental Information.

Locations along the rostral-caudal axis of the E16 brain were matched as described in Supplemental Information to account for gradients in the developing brain. Boxes for quantitation of the E16 brain were drawn to encompass the entire layer within the region (for example, lateral CP, IZ and VZ/SVZ) and the summation of CP, IZ, and VZ/SVZ boxes corresponded to the total cortex. For P7, images were taken of coronal sections from lateral regions of the somatosensory cortex of the anterior forebrain as described in Supplemental Information. Quantitation focused on the P7 neocortex (defined as the region above the corpus callosum white matter tracts). Boxes were drawn from the upper edge of the white matter tracts to the pial surface for analysis. For analysis of layers 2/3, 4, and 5/6, nuclei patterns were used to discern the layers and 3 boxes (200x100 μ m) were drawn within the layer, enabling analysis in the middle of each layer to avoid boundaries.

Data were analyzed from 3 or more brains per genotype. Antibody and Hoechst staining were used to quantify the following: the percentage of positively stained cells (number positively stained/total number Hoechst stained cells), cells/mm² (number positively stained per unit area), total cell number (total number positively stained in the region). The thickness of regions or layers was measured using Hoechst staining to define architectural boundaries and ImageJ to determine distance between boundaries.

Graphs and statistical analysis

Lines in dot plots show mean and the bars show standard error of the mean. For box plots, the box extends from the 25th to 75th percentiles, the line in the middle of the box is the median, and the boxes have Tukey whiskers. Comparison of two samples utilized two-tailed unpaired Student's t-tests. Datasets containing more than two samples were analyzed by one-way ANOVA with Tukey's post hoc correction for multiple samples.

Acknowledgements:

The authors gratefully acknowledge Dr. Michael Demetriou for *Mgat5* knockout mice. This work was supported in part by NSF IOS-2019400 (LAF), NSF CAREER Award IOS-1254060 (LAF), NIH NINDS T32 NS082174 (predoctoral fellowship to AY), and Brython Davis Fellowship (AY).

Author Contributions:

Conceptualization, A.R.Y., E.K., J.L.N., L.A.F.; Methodology, R.F.H., E.S.M., L.A.F.; Investigation, A.R.Y., E.K., B.G., J.N.H., N.S.L., J.L.N., M.S.; Resources, L.A.F.; Writing - Original Draft, A.R.Y.; Writing - Review and Editing, L.A.F.; Funding Acquisition, A.R.Y., L.A.F.; Supervision, L.A.F.

Declaration of Interests:

The authors declare no competing interests.

References

- Abbott, K. L. and J. M. Pierce (2010). "Lectin-based glycoproteomic techniques for the enrichment and identification of potential biomarkers." <u>Methods Enzymol</u> **480**: 461-476.
- Adams, T. N. G., A. Y. L. Jiang, N. S. Mendoza, C. C. Ro, D. H. Lee, A. P. Lee and L. A. Flanagan (2020). "Label-free enrichment of fate-biased human neural stem and progenitor cells." Biosens Bioelectron **152**: 111982.
- Bagnaninchi, P. O. and N. Drummond (2011). "Real-time label-free monitoring of adiposederived stem cell differentiation with electric cell-substrate impedance sensing." Proc Natl-Acad Sci USA 108(16): 6462-6467.
- Belinson, H., J. Nakatani, B. A. Babineau, R. Y. Birnbaum, J. Ellegood, M. Bershteyn, R. J. McEvilly, J. M. Long, K. Willert, O. D. Klein, N. Ahituv, J. P. Lerch, M. G. Rosenfeld and A. Wynshaw-Boris (2016). "Prenatal beta-catenin/Brn2/Tbr2 transcriptional cascade regulates adult social and stereotypic behaviors." Mol Psychiatry 21(10): 1417-1433.
- Breunig, J. J., J. I. Arellano, J. D. Macklis and P. Rakic (2007). "Everything that glitters isn't gold: a critical review of postnatal neural precursor analyses." <u>Cell Stem Cell</u> **1**(6): 612-627.
- Brockhausen, I., S. Narasimhan and H. Schachter (1988). "The biosynthesis of highly branched N-glycans: studies on the sequential pathway and functional role of N-acetylglucosaminyltransferases I, II, III, IV, V and VI." <u>Biochimie</u> **70**(11): 1521-1533.
- Dennis, J. W., K. S. Lau, M. Demetriou and I. R. Nabi (2009). "Adaptive regulation at the cell surface by N-glycosylation." <u>Traffic</u> **10**(11): 1569-1578.
- Dominguez, M. H., A. E. Ayoub and P. Rakic (2013). "POU-III transcription factors (Brn1, Brn2, and Oct6) influence neurogenesis, molecular identity, and migratory destination of upper-layer cells of the cerebral cortex." Cereb Cortex 23(11): 2632-2643.
- Feldcamp, L., J. S. Doucet, J. Pawling, M. P. Fadel, P. J. Fletcher, R. Maunder, J. W. Dennis and A. H. Wong (2016). "Mgat5 modulates the effect of early life stress on adult behavior and physical health in mice." <u>Behav Brain Res</u> **312**: 253-264.
- Granovsky, M., J. Fata, J. Pawling, W. J. Muller, R. Khokha and J. W. Dennis (2000). "Suppression of tumor growth and metastasis in Mgat5-deficient mice." <u>Nat Med</u> **6**(3): 306-312.
- Hamouda, H., M. Ullah, M. Berger, M. Sittinger, R. Tauber, J. Ringe and V. Blanchard (2013). "N-glycosylation profile of undifferentiated and adipogenically differentiated human bone marrow mesenchymal stem cells: towards a next generation of stem cell markers." <u>Stem Cells Dev 22</u>(23): 3100-3113.
- He, W., C. Ingraham, L. Rising, S. Goderie and S. Temple (2001). "Multipotent stem cells from the mouse basal forebrain contribute GABAergic neurons and oligodendrocytes to the cerebral cortex during embryogenesis." J Neurosci **21**(22): 8854-8862.
- Heiskanen, A., T. Hirvonen, H. Salo, U. Impola, A. Olonen, A. Laitinen, S. Tiitinen, S. Natunen, O. Aitio, H. Miller-Podraza, M. Wuhrer, A. M. Deelder, J. Natunen, J. Laine, P. Lehenkari, J. Saarinen, T. Satomaa and L. Valmu (2009). "Glycomics of bone marrow-derived mesenchymal stem cells can be used to evaluate their cellular differentiation stage." Glycoconj J 26(3): 367-384.
- Hildebrandt, C., H. Buth, S. Cho, Impidjati and H. Thielecke (2010). "Detection of the osteogenic differentiation of mesenchymal stem cells in 2D and 3D cultures by electrochemical impedance spectroscopy." J Biotechnol **148**(1): 83-90.
- Hirabayashi, J., H. Tateno, T. Shikanai, K. F. Aoki-Kinoshita and H. Narimatsu (2015). "The Lectin Frontier Database (LfDB), and data generation based on frontal affinity chromatography." <u>Molecules</u> **20**(1): 951-973.
- Ioffe, E. and P. Stanley (1994). "Mice lacking N-acetylglucosaminyltransferase I activity die at mid-gestation, revealing an essential role for complex or hybrid N-linked carbohydrates." <u>Proc Natl Acad Sci U S A</u> 91(2): 728-732.

- Labeed, F. H., J. Lu, H. J. Mulhall, S. A. Marchenko, K. F. Hoettges, L. C. Estrada, A. P. Lee, M. P. Hughes and L. A. Flanagan (2011). "Biophysical characteristics reveal neural stem cell differentiation potential." <u>PLoS One</u> **6**(9): e25458.
- Lee, A. P., M. Aghaamoo, T. N. G. Adams and L. A. Flanagan (2018). "It's electric: when technology gives a boost to stem cell science." <u>Current Stem Cell Reports</u> **4**(2): 116-126.
- Lee, S. U., A. Grigorian, J. Pawling, I. J. Chen, G. Gao, T. Mozaffar, C. McKerlie and M. Demetriou (2007). "N-glycan processing deficiency promotes spontaneous inflammatory demyelination and neurodegeneration." <u>J Biol Chem</u> **282**(46): 33725-33734.
- Luciano, M., J. E. Huffman, A. Arias-Vasquez, A. A. Vinkhuyzen, C. M. Middeldorp, I. Giegling, A. Payton, G. Davies, L. Zgaga, J. Janzing, X. Ke, T. Galesloot, A. M. Hartmann, W. Ollier, A. Tenesa, C. Hayward, M. Verhagen, G. W. Montgomery, J. J. Hottenga, B. Konte, J. M. Starr, V. Vitart, P. E. Vos, P. A. Madden, G. Willemsen, H. Konnerth, M. A. Horan, D. J. Porteous, H. Campbell, S. H. Vermeulen, A. C. Heath, A. Wright, O. Polasek, S. B. Kovacevic, N. D. Hastie, B. Franke, D. I. Boomsma, N. G. Martin, D. Rujescu, J. F. Wilson, J. Buitelaar, N. Pendleton, I. Rudan and I. J. Deary (2012). "Genome-wide association uncovers shared genetic effects among personality traits and mood states." Am J Med Genet B Neuropsychiatr Genet 159B(6): 684-695.
- Males, A., L. Raich, S. J. Williams, C. Rovira and G. J. Davies (2017). "Conformational analysis of the mannosidase inhibitor kifunensine: a quantum mechanical and structural approach." <u>ChemBioChem</u> **18**: 1496-1501.
- Metzler, M., A. Gertz, M. Sarkar, H. Schachter, J. W. Schrader and J. D. Marth (1994). "Complex asparagine-linked oligosaccharides are required for morphogenic events during post-implantation development." <u>EMBO J</u> **13**(9): 2056-2065.
- Nourse, J. L., J. L. Prieto, A. R. Dickson, J. Lu, M. M. Pathak, F. Tombola, M. Demetriou, A. P. Lee and L. A. Flanagan (2014). "Membrane biophysics define neuron and astrocyte progenitors in the neural lineage." <u>Stem Cells</u> **32**(3): 706-716.
- Oguri, S. (2005). "Analysis of sugar chain-binding specificity of tomato lectin using lectin blot: recognition of high mannose-type N-glycans produced by plants and yeast." <u>Glycoconj J</u> **22**(7-9): 453-461.
- Ohtsubo, K. and J. D. Marth (2006). "Glycosylation in cellular mechanisms of health and disease." Cell 126(5): 855-867.
- Pinho, S. S., C. A. Reis, J. Paredes, A. M. Magalhaes, A. C. Ferreira, J. Figueiredo, W. Xiaogang, F. Carneiro, F. Gartner and R. Seruca (2009). "The role of N-acetylglucosaminyltransferase III and V in the post-transcriptional modifications of Ecadherin." <u>Hum Mol Genet</u> **18**(14): 2599-2608.
- Rowitch, D. H. and A. R. Kriegstein (2010). "Developmental genetics of vertebrate glial-cell specification." <u>Nature</u> **468**(7321): 214-222.
- Schachter, H. (2001). "Congenital disorders involving defective N-glycosylation of proteins." <u>Cell Mol Life Sci</u> **58**(8): 1085-1104.
- Scott, H. and V. M. Panin (2014). "The role of protein N-glycosylation in neural transmission." Glycobiology **24**(5): 407-417.
- Soleimani, L., J. C. Roder, J. W. Dennis and T. Lipina (2008). "Beta N-acetylglucosaminyltransferase V (Mgat5) deficiency reduces the depression-like phenotype in mice." Genes Brain Behav **7**(3): 334-343.
- Sugitani, Y., S. Nakai, O. Minowa, M. Nishi, K. Jishage, H. Kawano, K. Mori, M. Ogawa and T. Noda (2002). "Brn-1 and Brn-2 share crucial roles in the production and positioning of mouse neocortical neurons." <u>Genes Dev</u> **16**(14): 1760-1765.
- Taverna, E., M. Gotz and W. B. Huttner (2014). "The cell biology of neurogenesis: toward an understanding of the development and evolution of the neocortex." <u>Annu Rev Cell Dev Biol</u> **30**: 465-502.
- Terashima, M., M. Amano, T. Onodera, S. Nishimura and N. Iwasaki (2014). "Quantitative glycomics monitoring of induced pluripotent- and embryonic stem cells during neuronal differentiation." <u>Stem Cell Res</u> **13**(3 Pt A): 454-464.

- Wang, Y., H. Schachter and J. D. Marth (2002). "Mice with a homozygous deletion of the Mgat2 gene encoding UDP-N-acetylglucosamine:alpha-6-D-mannoside beta1,2-N-acetylglucosaminyltransferase II: a model for congenital disorder of glycosylation type IIa." <u>Biochim Biophys Acta</u> **1573**(3): 301-311.
- Yale, A. R., J. L. Nourse, K. R. Lee, S. N. Ahmed, J. Arulmoli, A. Y. L. Jiang, L. P. McDonnell, G. A. Botten, A. P. Lee, E. S. Monuki, M. Demetriou and L. A. Flanagan (2018). "Cell surface N-glycans influence electrophysiological properties and fate potential of neural stem cells." Stem Cell Reports 11(4): 869-882.
- Zhao, Y., T. Nakagawa, S. Itoh, K. Inamori, T. Isaji, Y. Kariya, A. Kondo, E. Miyoshi, K. Miyazaki, N. Kawasaki, N. Taniguchi and J. Gu (2006). "N-acetylglucosaminyltransferase III antagonizes the effect of N-acetylglucosaminyltransferase V on alpha3beta1 integrin-mediated cell migration." <u>J Biol Chem</u> **281**(43): 32122-32130.
- Zhao, Y. Y., M. Takahashi, J. G. Gu, E. Miyoshi, A. Matsumoto, S. Kitazume and N. Taniguchi (2008). "Functional roles of N-glycans in cell signaling and cell adhesion in cancer." <u>Cancer Sci</u> **99**(7): 1304-1310.

Figures and Legends

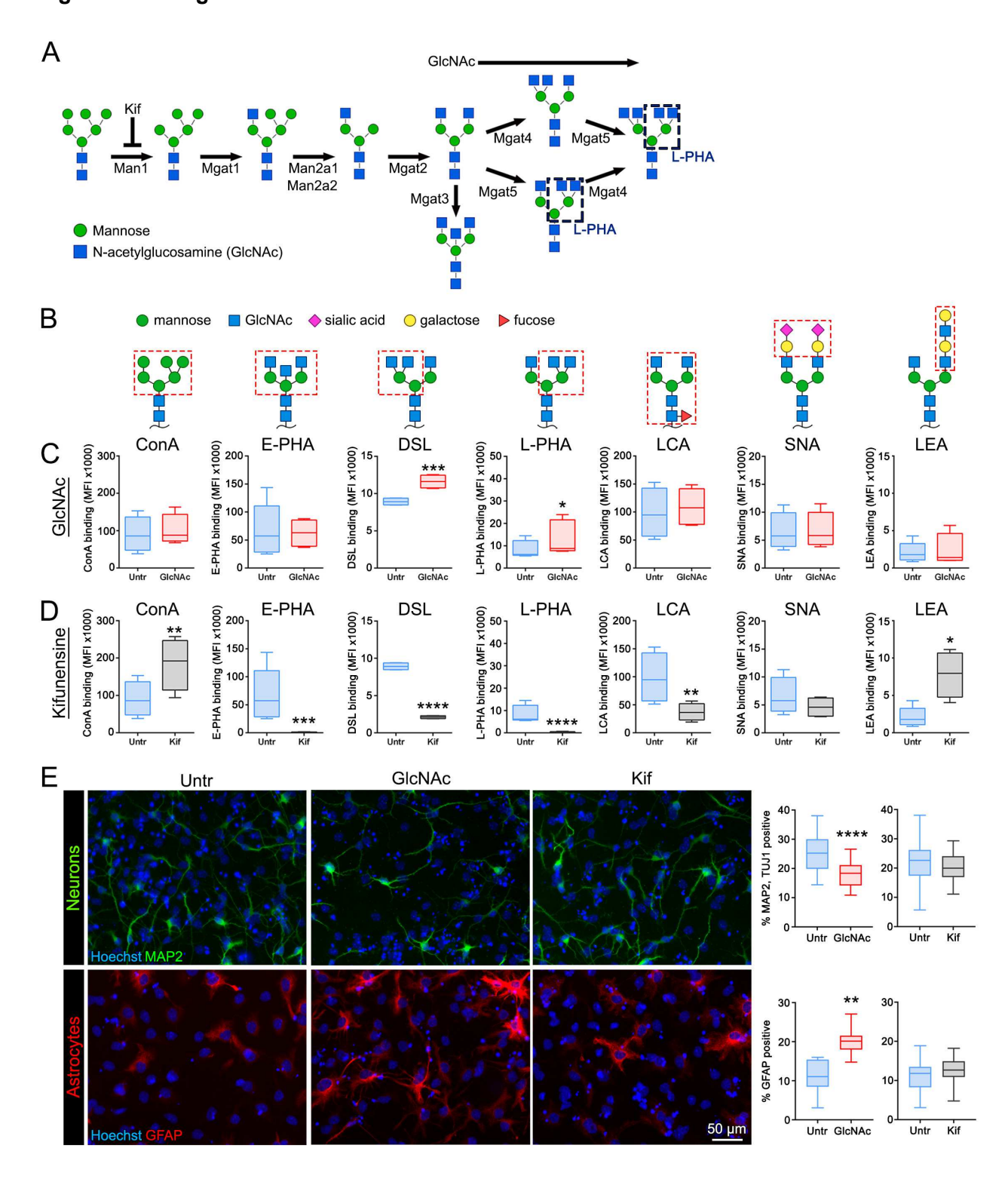


Figure 1. Kifunensine treatment alters multiple N-glycan species and does not affect neuron and astrocyte differentiation

- (A) Schematic of N-glycans formed by glycosylation enzymes, culminating in highly branched N-glycans with β1-6 branches recognized by L-PHA. Kif blocks MAN1 while GlcNAc provides substrate that enhances branched N-glycan formation.
- (B) N-glycans, symbols denote particular sugar moieties. Boxed regions indicate structures recognized by lectins ConA, E-PHA, DSL, L-PHA, LCA, SNA, LEA.
- (C) E12 NSPCs treated with GlcNAc had significantly more branched N-glycans detected by DSL (p=0.0001) and L-PHA (p=0.015) compared to untreated (Untr) controls.
- (D) Kif treated E12 NSPCs had higher levels of N-glycans detected by ConA (p=0.0025) and LEA (p=0.04), but lower levels of those that bind E-PHA (p=0.0002), DSL (p<0.0001), L-PHA (p<0.0001), and LCA (p=0.001).
- (E) E12 NSPCs treated with GlcNAc, Kif or untreated controls were differentiated and immunostained to detect neurons (microtubule associated protein 2, MAP2, and TuJ1) or astrocytes (glial fibrillary acidic protein, GFAP). GlcNAc treatment reduced neuron formation (p<0.0001) and increased generation of astrocytes (p=0.0014) while Kif had no effect. All nuclei were stained with Hoechst. Analyses used unpaired two-tailed Student's t-test, N≥3 independent biological repeats. Box plots show median with Tukey whiskers, *p<0.05, **p<0.01, ****p<0.001.

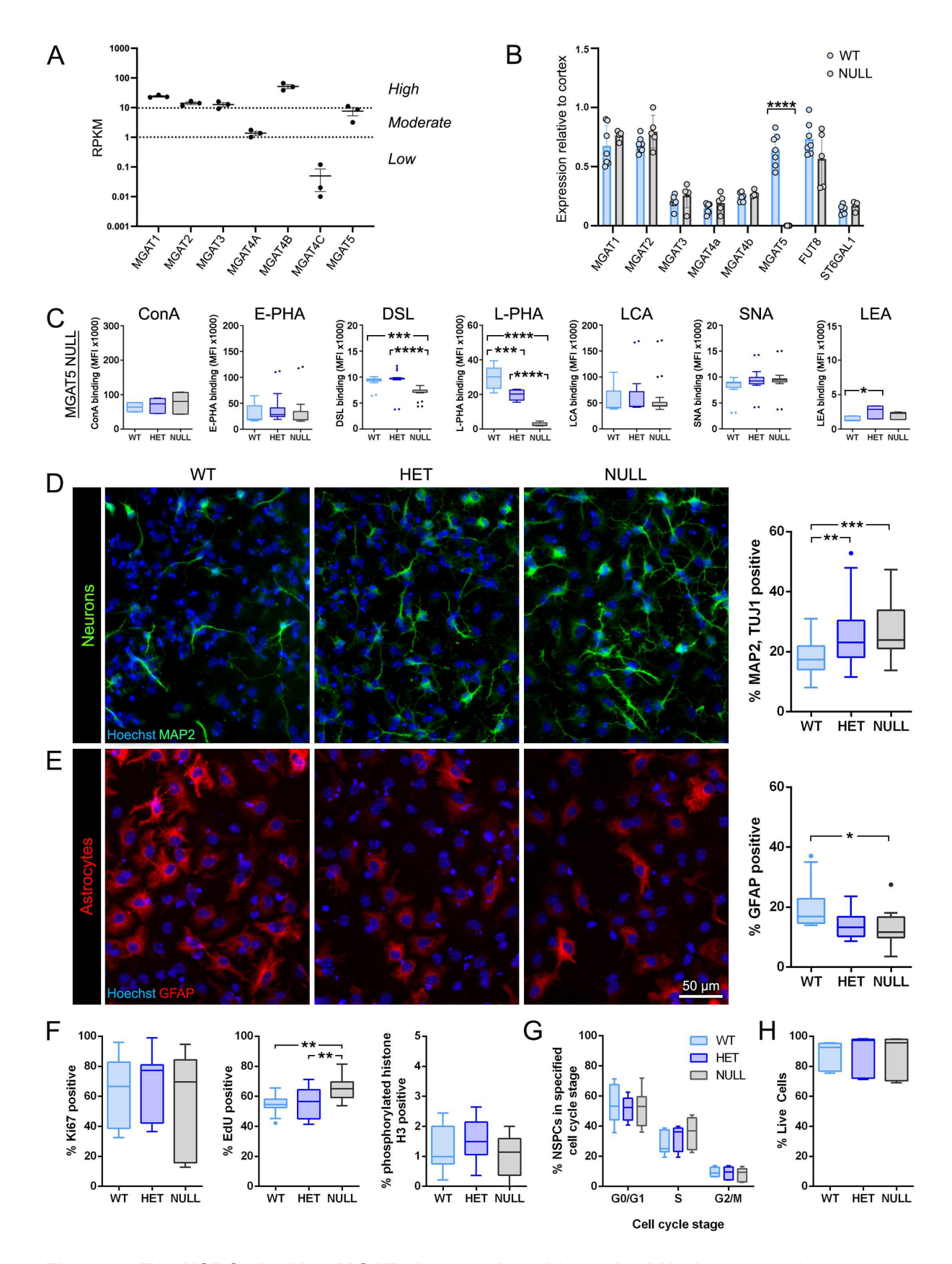


Figure 2. E12 NSPCs lacking MGAT5 have reduced branched N-glycans and generate

more neurons and fewer astrocytes in vitro.

- (A) RNAseq analysis of E12 NSPCs shows expression levels of N-acetylglucosaminyltransferases. Data are from 3 independent biological repeats and the scatterplot displays average RPKM values for each enzyme (error is SEM). Genes are clustered into high (>10 RPKM), moderate (1–10 RPKM), and low to no (<1 RPKM) expression. For comparison, beta-actin and the stem cell marker Prominin 1 (CD133) are highly expressed, the gamma secretase involved in Notch signaling is moderately expressed, and the muscle marker MyoD shows low to no expression.
- (B) Comparison of glycosylation enzyme transcripts by qRT-PCR shows loss of *Mgat5* in null NSPCs (p<0.0001). Expression is relative to control total cortex, **error bars show standard deviation**, and WT and null were compared by unpaired two-tailed Student's t-test.
- (C) Analysis of E12 NSPCs from Mgat5 WT, heterozygous (het) and null mice showed that het (p=0.0004) and null (p<0.0001) NSPCs exhibited lower levels of β 1-6 branched N-glycans detected by L-PHA compared to WT cells. Null cells had lower levels of β 1-4 branched N-glycans detected by DSL compared to WT (p=0.0001) and het (p<0.0001). Het NSPCs showed a slight increase in polylactosamine detected by LEA (p=0.019).
- (D) Compared to WT, *Mgat5* het (p=0.008) and null (p=0.0009) E12 NSPCs differentiated into more neurons. All nuclei were stained with Hoechst in D and E.
- (E) The percentage of GFAP-positive astrocytes formed by null E12 NSPCs was significantly reduced compared to WT (p=0.027).
- (F) No difference in Ki67 or phosphorylated histone H3 labeling was observed. However, *Mgat5* E12 null NSPCs had significantly increased EdU incorporation compared to WT (p=0.002) and heterozygous (p=0.006).
- (G) Cell cycle analysis by propidium iodide labeling and flow cytometry revealed no significant difference in the proportion of cells in G_0/G_1 , S, or G_2/M phase among WT, heterozygous, and null E12 NSPCs.
- (H) The percentage of live cells was assessed by co-staining with propidium iodide and calcein-AM. No difference in cell viability was detected between the *Mgat5* WT, het and null NSPCs. Analyses used one-way ANOVA, Tukey's *post hoc*, N≥3 independent biological repeats. Box plots show median with Tukey whiskers, *p<0.05, **p<0.01, ***p<0.001, ****p<0.0001.

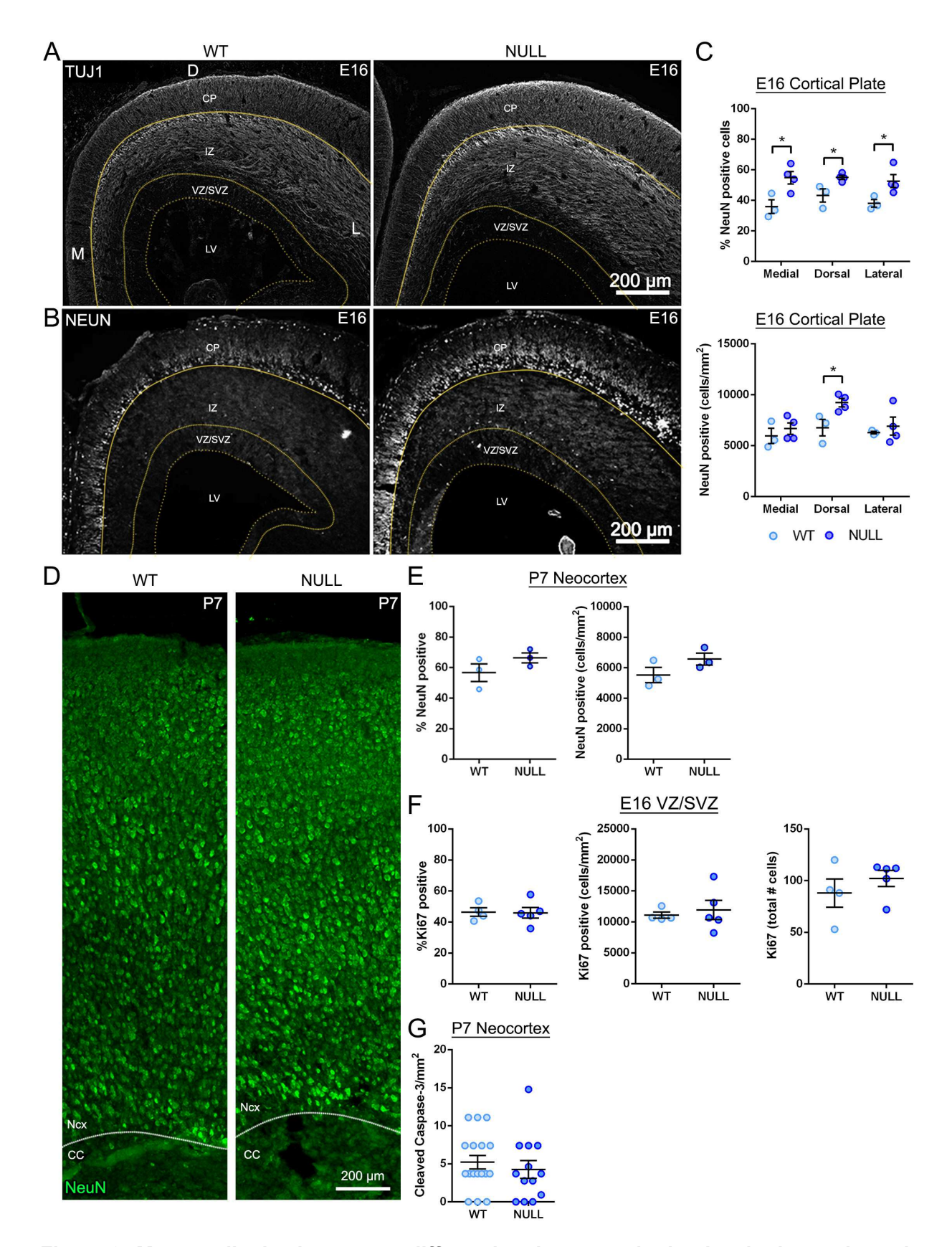


Figure 3. Mgat5 null mice have more differentiated neurons in the developing embryonic

cortex but no change in cell proliferation or death.

- (A) Greater TuJ1 neuronal staining is evident in coronal sections of E16 null brain compared to WT. Sections show medial (M), dorsal (D), and lateral (L) regions and CP, IZ, VZ/SVZ, and lateral ventricle (LV).
- (B) Coronal sections show enhanced NeuN in the Mgat5 null brain CP at E16.
- (C) Quantification shows a significant increase in the percentage of NeuN positive cells in the *Mgat5* null brain CP compared to WT in medial (p=0.027), dorsal (p=0.029), and lateral (p=0.049) regions. There was a significant increase in the number of NeuN positive cells per area (cells/ mm²) in the *Mgat5* null dorsal CP compared to WT (p=0.031).
- (D) P7 coronal sections of WT and *Mgat5* null brains were immunostained to detect NeuN. Images show the neocortex (Ncx) and corpus callosum (CC) in lateral cortical regions.
- (E) There was a non-significant increase in the percentage and number per mm² of NeuN positive cells in *Mgat5* null neocortex compared to WT at P7.
- (F) Staining with Ki67 in the E16 lateral VZ/SVZ showed no difference between WT and null brains.
- (G) There was no difference in the number of cleaved Caspase-3 positive cells per mm² in the P7 neocortex between WT and *Mgat5* null brains. The lateral ventricle is toward the bottom of images, analyses used unpaired two-tailed Student's t-test WT vs. null, N=3-4 mice per genotype and for Caspase-3 staining multiple fields per animal. Lines and error bars in dot plots show mean with SEM, respectively, *p<0.05.

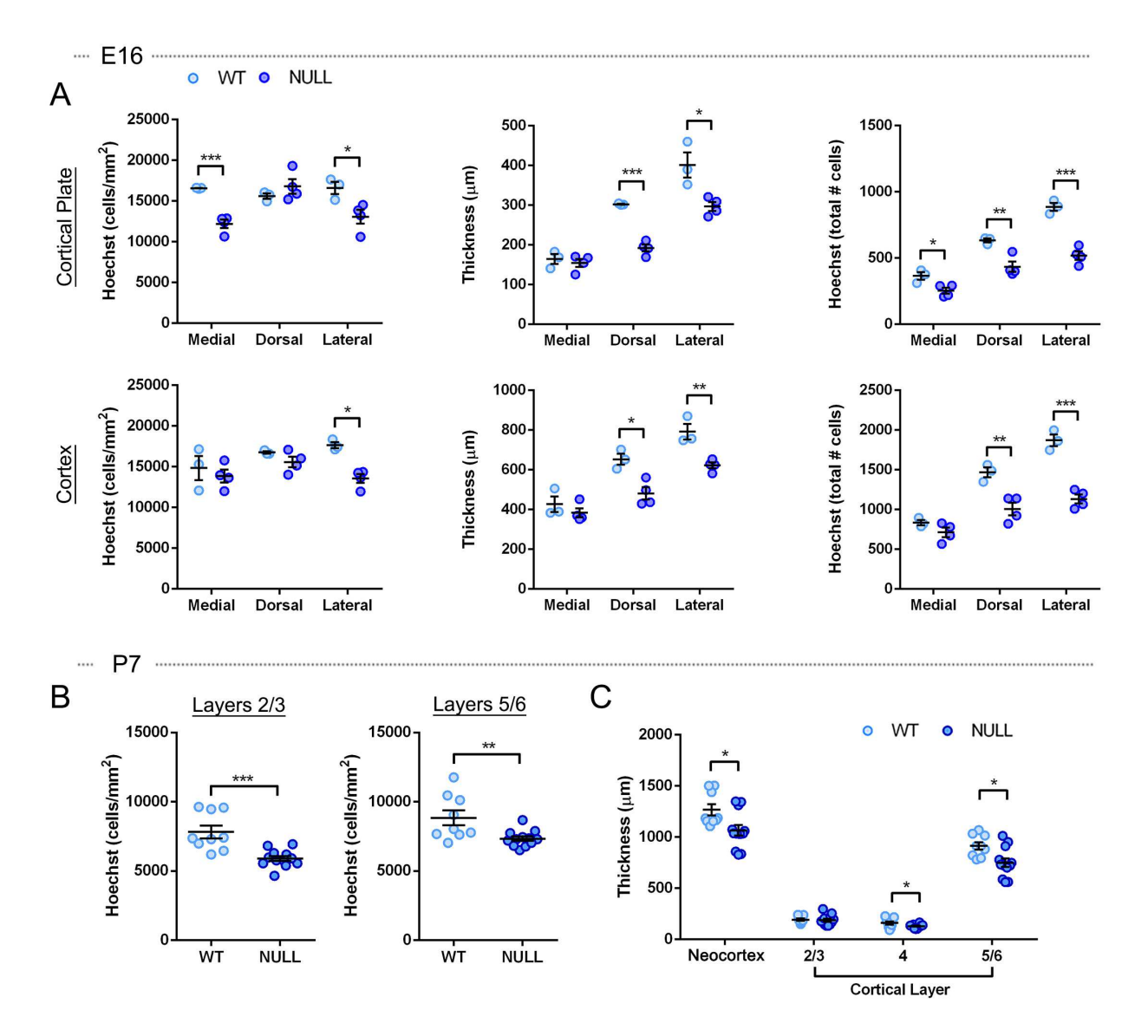


Figure 4. Mgat5 null brains display decreased cell numbers and thickness.

(A) At E16, cell density (cells/mm²) was significantly decreased in the medial (p=0.0009) and lateral (p=0.032) null CP and in the null lateral cortex (p=0.003) compared to WT. In Mgat5 null brains, the thickness of the CP and cortex were reduced compared to WT: CP dorsal (p=0.0001), CP lateral (p=0.017), cortex dorsal (p=0.011), cortex lateral (p=0.006). The total number of cells was reduced in the medial (p=0.025), dorsal (p=0.008), and lateral (p=0.0005) null CP and in the null dorsal (p=0.008) and lateral (p=0.0004) cortex compared to WT.

(B) At P7, the number of cells per mm² in Mgat5 null was significantly reduced in layers 2/3 (p=0.0004) and layers 5/6 (p=0.007) compared to WT.

(C) Thickness of the neocortex was significantly reduced in the *Mgat5* null brain compared to WT at P7 (p=0.018). The thickness of layer 4 (p=0.0496) and layers 5/6 (p=0.01) was significantly reduced in the *Mgat5* null brain compared to WT. Analyses used unpaired two-tailed Student's t-test WT vs. null, N=3-5 mice per genotype and, for P7, 3 regions per animal. Lines and error bars in dot plots show mean with SEM, respectively, *p<0.05, **p<0.01, ***p<0.001.

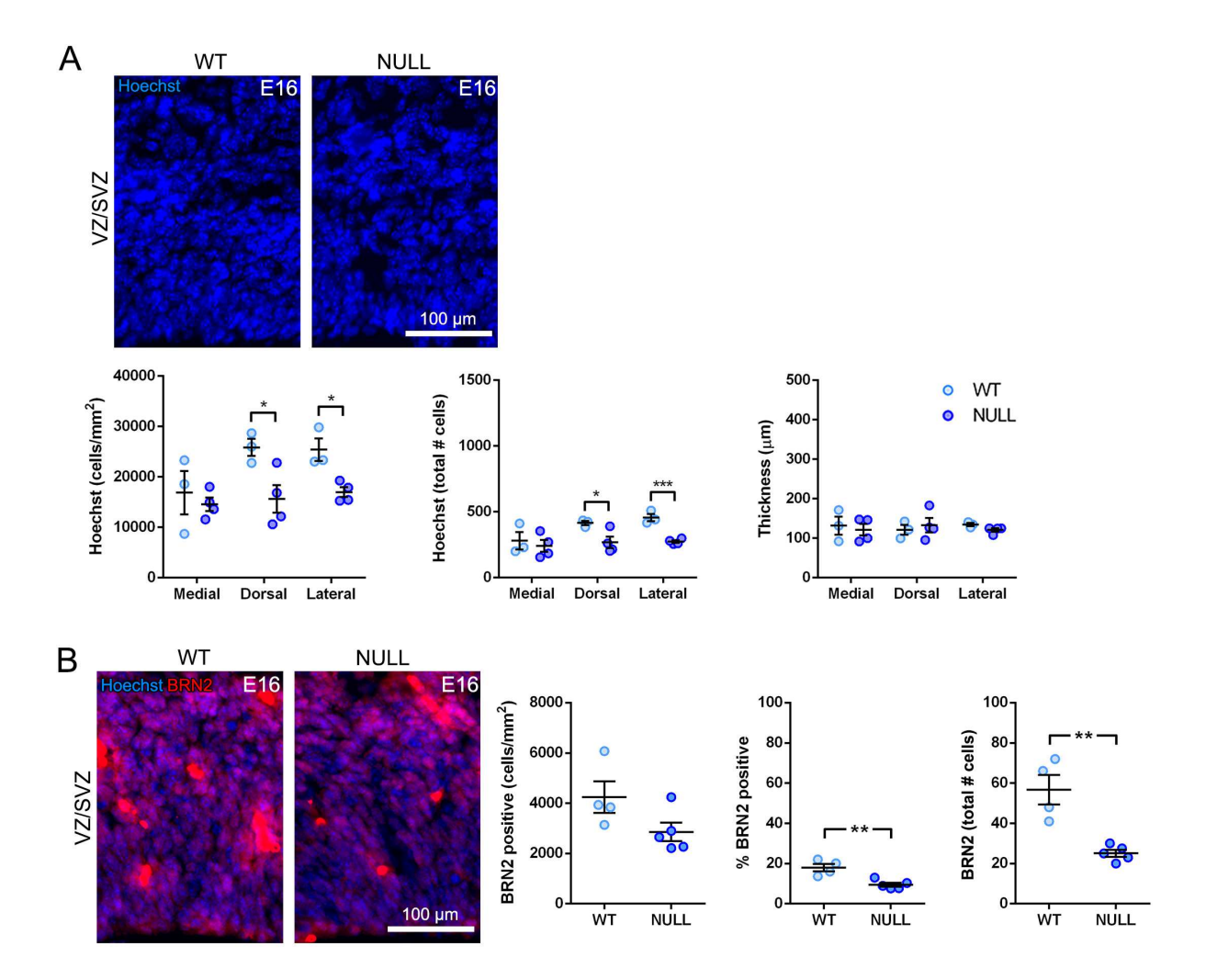


Figure 5. MGAT5 deficiency causes depletion of embryonic VZ/SVZ cells and upper layer neuron progenitors.

- (A) Number of Hoechst-stained cells per mm² was significantly decreased in the E16 *Mgat5* null dorsal (p=0.034) and lateral (p=0.012) VZ/SVZ compared to WT. The total number of Hoechst-stained cells was significantly reduced in the *Mgat5* null dorsal (p=0.037) and lateral (p=0.0009) VZ/SVZ compared to WT. The thickness of the VZ/SVZ did not differ between WT and null brains.
- (B) The percentage (p=0.004) and total number (p=0.002) of BRN2-positive upper layer neuron progenitors in the dorsal VZ/SVZ was reduced in E16 *Mgat5* nulls compared to WT. All nuclei were stained with Hoechst, the ventricle is toward the bottom of the images. Analyses used unpaired two-tailed Student's t-test WT vs. null, N=3-5 mice per genotype. Lines and error bars in dot plots show mean with SEM, respectively, *p<0.05, **p<0.01, ***p<0.001.

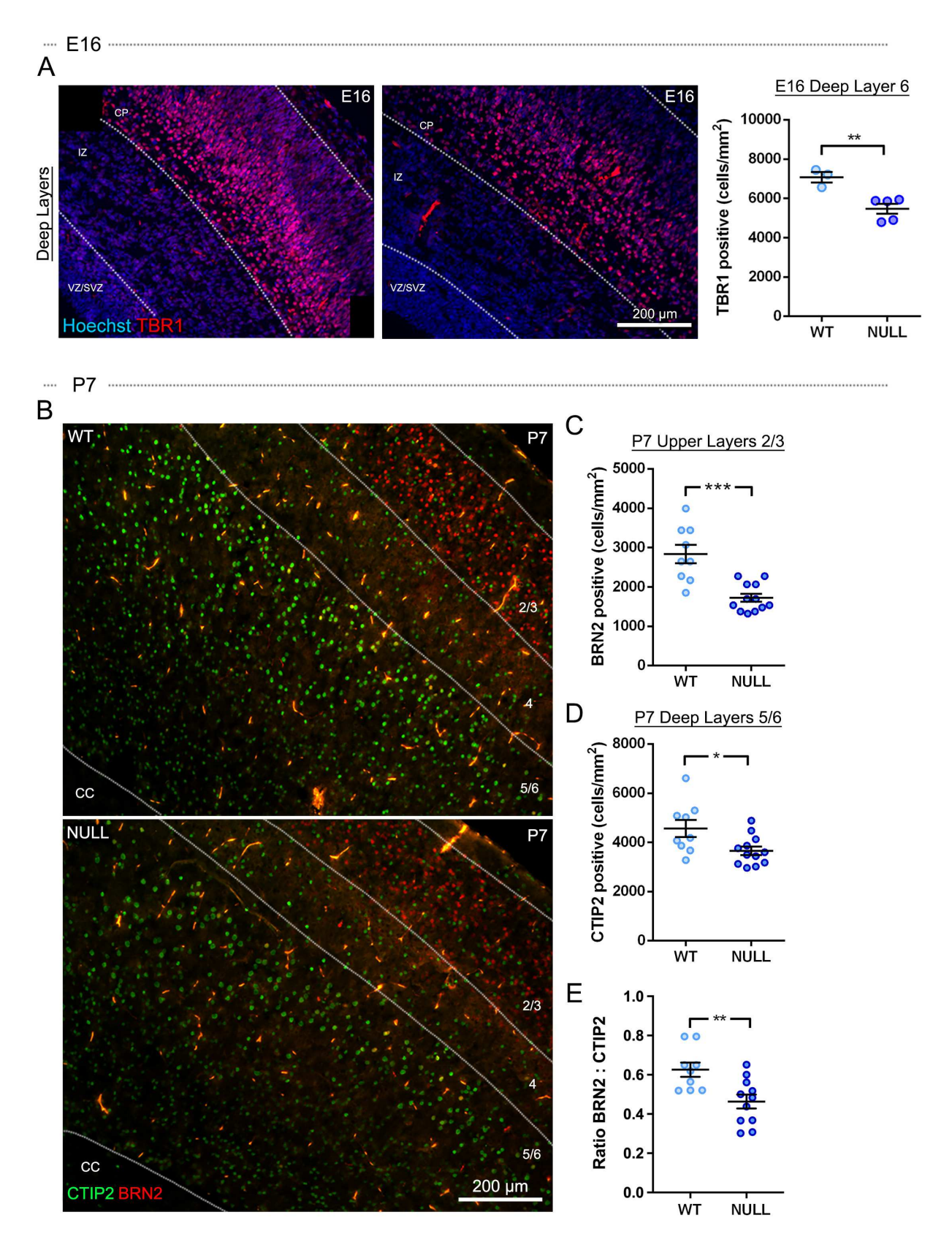


Figure 6. Progenitor depletion in the absence of MGAT5 causes greater effects on later

born upper layer neurons.

- (A) Coronal sections of E16 brain were immunostained to detect deep layer 6 neuron marker TBR1. The ventricle is toward the bottom left corner of the image. TBR1-positive neurons were significantly reduced (p=0.007) in the *Mgat5* null lateral CP compared to WT.
- (B) Coronal sections of P7 WT and *Mgat5* null brains were immunostained to detect the upper layer neuron marker BRN2 (red) and the deep layer 5/6 neuron marker CTIP2 (green). The ventricle is toward the bottom left corners of the images.
- (C) BRN2-positive upper layer 2/3 neurons were significantly reduced in *Mgat5* null neocortex compared to WT at P7 (p=0.0001).
- (D) Deep layer 5/6 neurons detected by CTIP2 were significantly reduced in the *Mgat5* null brain compared to WT (p=0.02).
- (E) There was a significant decrease in the ratio of BRN2:CTIP2 neurons in the *Mgat5* null brain compared to WT (p=0.003) at P7. All nuclei were stained with Hoechst and analyses used unpaired two-tailed Student's t-test WT vs. null, N=3-5 mice per genotype and 3 regions per animal for P7. Lines and error bars in dot plots show mean with SEM, respectively, *p<0.05, **p<0.01, ***p<0.001.

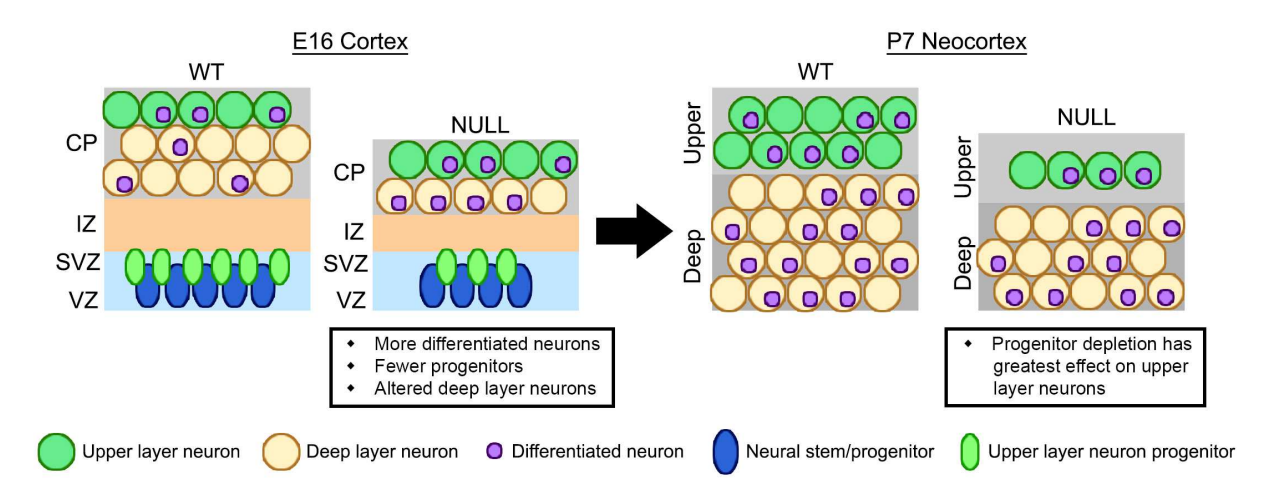


Figure 7. Model: accelerated neuronal differentiation and progenitor depletion during cortical development in the *Mgat5* null brain.

Our data suggest a model in which *Mgat5* null NSPCs rapidly form fully differentiated neurons, leading to an increase in NeuN-expressing cells (purple nuclei) in the *Mgat5* null CP at E16. Rapid neuronal differentiation in *Mgat5* nulls leads to progenitor depletion, reducing VZ/SVZ cell numbers and upper layer neuron progenitors. Progenitor reduction leads to a decrease in deep layer neurons and cortical thickness at E16 in *Mgat5* nulls. By P7, the *Mgat5* null brain has decreased cortical cell numbers and thickness and a more profound reduction in later born upper layer neurons compared to earlier born deep layers. Thus, loss of MGAT5 leads to a more rapid production of differentiated neurons that depletes progenitors, causing reduced cell numbers and cortical thickness and more severe reductions in neurons formed later in development.

Stem Cell Reports

Supplemental Information

Regulation of neural stem cell differentiation and brain development by MGAT5-mediated N-glycosylation

Andrew R. Yale^{1,2,3}, Estelle Kim^{2,3}, Brenda Gutierrez^{1,2,3}, J. Nicole Hanamoto^{2,3}, Nicole S. Lav³, Jamison L. Nourse^{2,3}, Marc Salvatus³, Robert F. Hunt^{1,3}, Edwin S. Monuki^{3,4}, Lisa A. Flanagan*^{1,2,3,5}

¹Department of Anatomy & Neurobiology, University of California Irvine, Irvine, CA 92697, USA

²Department of Neurology, University of California Irvine, Irvine, CA 92697, USA

³Sue & Bill Gross Stem Cell Research Center, University of California Irvine, Irvine, CA 92697, USA

⁴Department of Pathology and Laboratory Medicine, University of California Irvine, Irvine, CA 92697, USA

⁵Department of Biomedical Engineering, University of California Irvine, Irvine, CA 92697, USA

*Correspondence: <u>lisa.flanagan@uci.edu</u>

Supplemental Figures

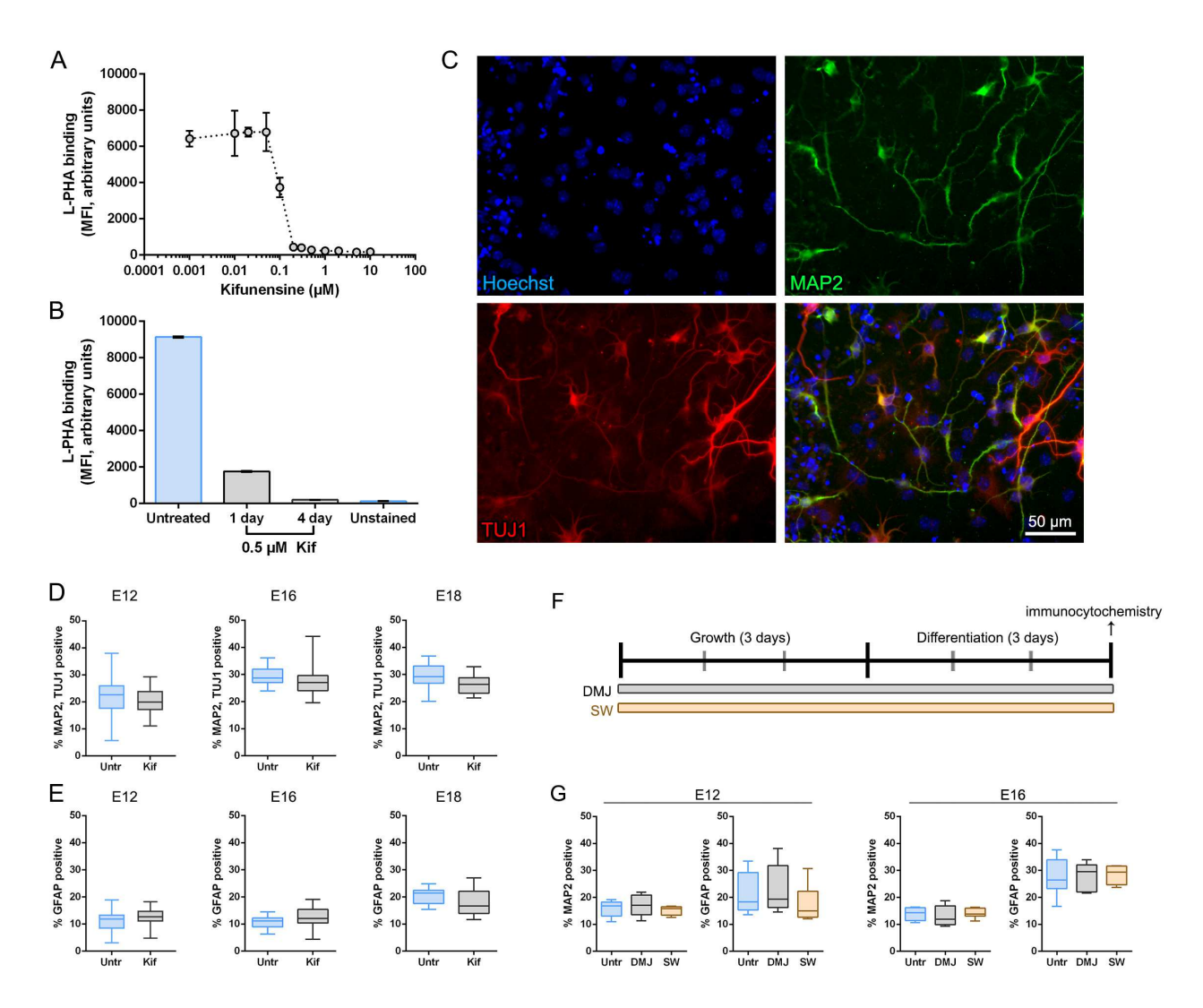


Figure S1. Blocking enzymes early in the branching pathway does not alter NSPC differentiation (related to Figure 1).

- (A) E12 NSPCs were treated for 4 days with varying doses of Kifunensine (Kif) (μM: 0.001, 0.01, 0.02, 0.05, 0.1, 0.2, 0.3, 0.5, 1, 2, 5, 10). At the conclusion of Kif treatment, NSPCs were labeled with L-PHA to detect highly branched N-glycans and analyzed by flow cytometry. The 0.5 μM Kif dose effectively disrupted formation of highly branched N-glycans and was used in subsequent experiments. N=3 independent biological repeats and error bars indicate SEM.
- (B) E12 NSPCs were treated with $0.5~\mu M$ Kif for 1 or 4 days and highly branched N-glycans analyzed by flow cytometry with L-PHA. Treatment for 4 days resulted in a greater decrease in L-PHA staining compared to treatment for 1 day. N=1 and error bars indicate SEM of technical replicates.
- (C) E12 NSPCs were differentiated for 3 days and co-immunostained to detect neuronal markers MAP2 (green) and TuJ1 (red). All nuclei were stained with Hoechst (blue). Quantitation of neurons in culture was based on co-labeling with both markers.
- (D, E) NSPCs isolated from E12, E16, and E18 embryonic cortices were treated with 0.5 μM Kif for 4 days then differentiated for 3 days and immunostained for markers of neurons in D (MAP2, TuJ1) or astrocytes in E (GFAP). There was no significant difference in the generation of MAP2/

TuJ1-positive neurons or GFAP-positive astrocytes between untreated control (Untr) and Kif treated NSPCs from any of the embryonic ages. The E12 data are as shown in Figure 1. (F) Schematic representing the design for experiments using the mannosidase inhibitors deoxymannojirimycin (DMJ) and swainsonine (SW). E12 or E16 NSPCs were treated with 1 μ M DMJ or 500 nM SW for 3 days in growth medium as undifferentiated cells and 3 days in differentiation medium. After differentiation, the cells were analyzed by immunocytochemistry to detect neurons and astrocytes.

(G) There was no significant difference in the generation of MAP2-positive neurons or GFAP-positive astrocytes from E12 or E16 NSPCs when treated with either DMJ or SW. All analyses used one-way ANOVA, Tukey's post hoc, N=3 independent biological repeats. Box plots show median with Tukey whiskers.

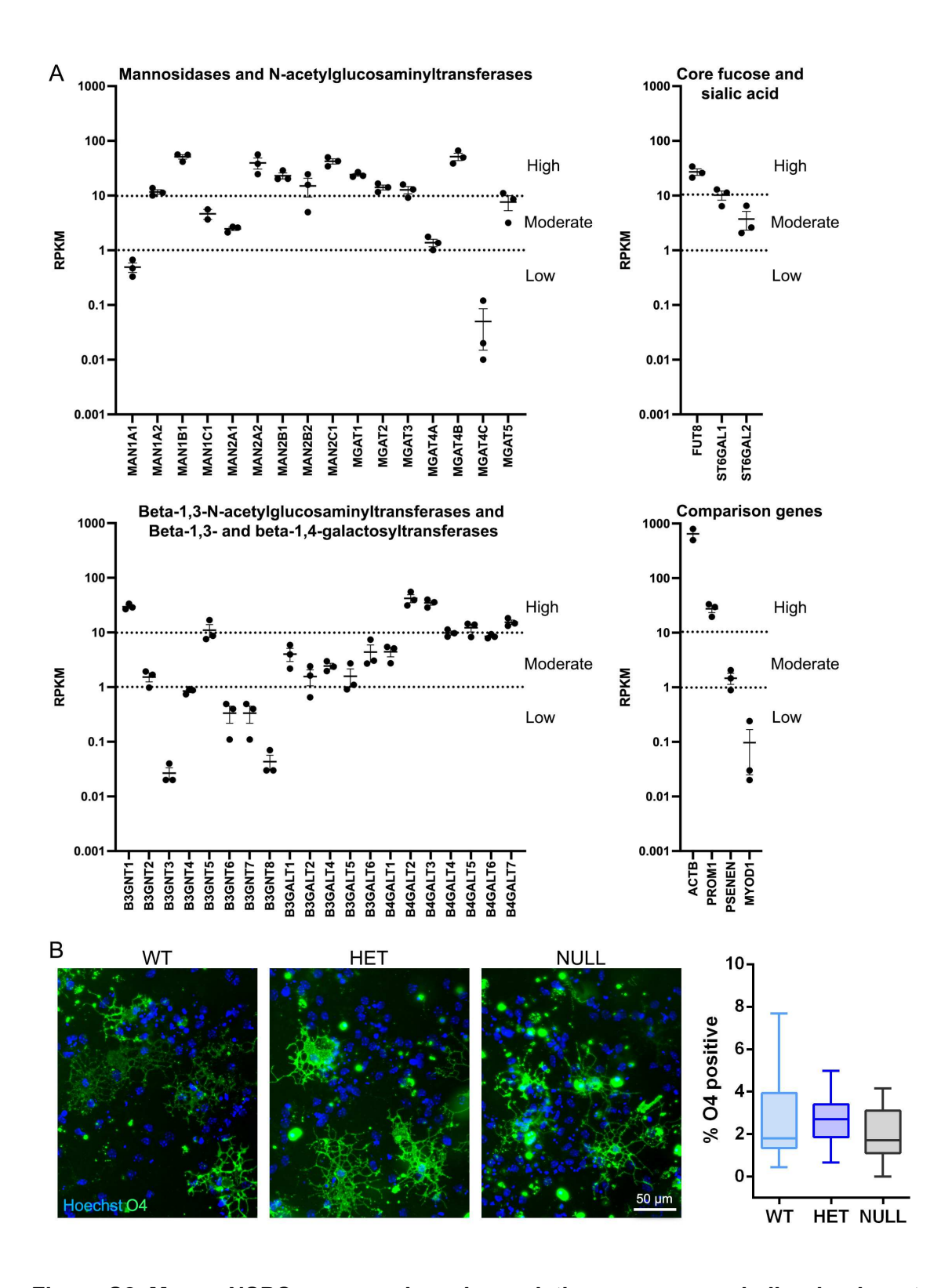


Figure S2. Mouse NSPCs express key glycosylation enzymes and oligodendrocyte differentiation is not significantly affected by loss of MGAT5 (related to Figure 2).

(A) RNAseq analysis of E12 mouse NSPCs reveals expression levels of glycosylation enzymes affecting cell surface N-glycans detected by ConA (high mannose, relates to Mannosidases), E-PHA (MGAT3), DSL (MGAT4A-C), L-PHA (MGAT5), LCA (FUT8), SNA (ST6GAL1-2), and LEA

(polylactosamine, B3GNT1-8, B3GALT1-6, B4GALT1-7). Data are from 3 independent biological repeats and the scatterplot displays average RPKM values for each enzyme (error is SEM). Genes are clustered into three categories: high (>10 RPKM), moderate (1–10 RPKM), and low to no (<1 RPKM) expression. Dotted lines indicate 10 RPKM and 1 RPKM boundaries. For comparison, beta-actin and the stem cell marker Prominin 1 (CD133) fall in the highly expressed category, the gamma secretase involved in Notch signaling is moderately expressed, and the muscle marker MyoD shows low to no expression.

(B) *Mgat5* WT, heterozygous, and null E12 NSPCs were differentiated for 7 days *in vitro* and immunostained to detect the oligodendrocyte marker O4 (green). Quantitation of cells expressing O4 indicates no difference in the formation of oligodendrocytes from WT, heterozygous, and null NSPCs. Analysis used one-way ANOVA, Tukey's post hoc, N≥3 independent biological repeats. Box plots show median with Tukey whiskers.

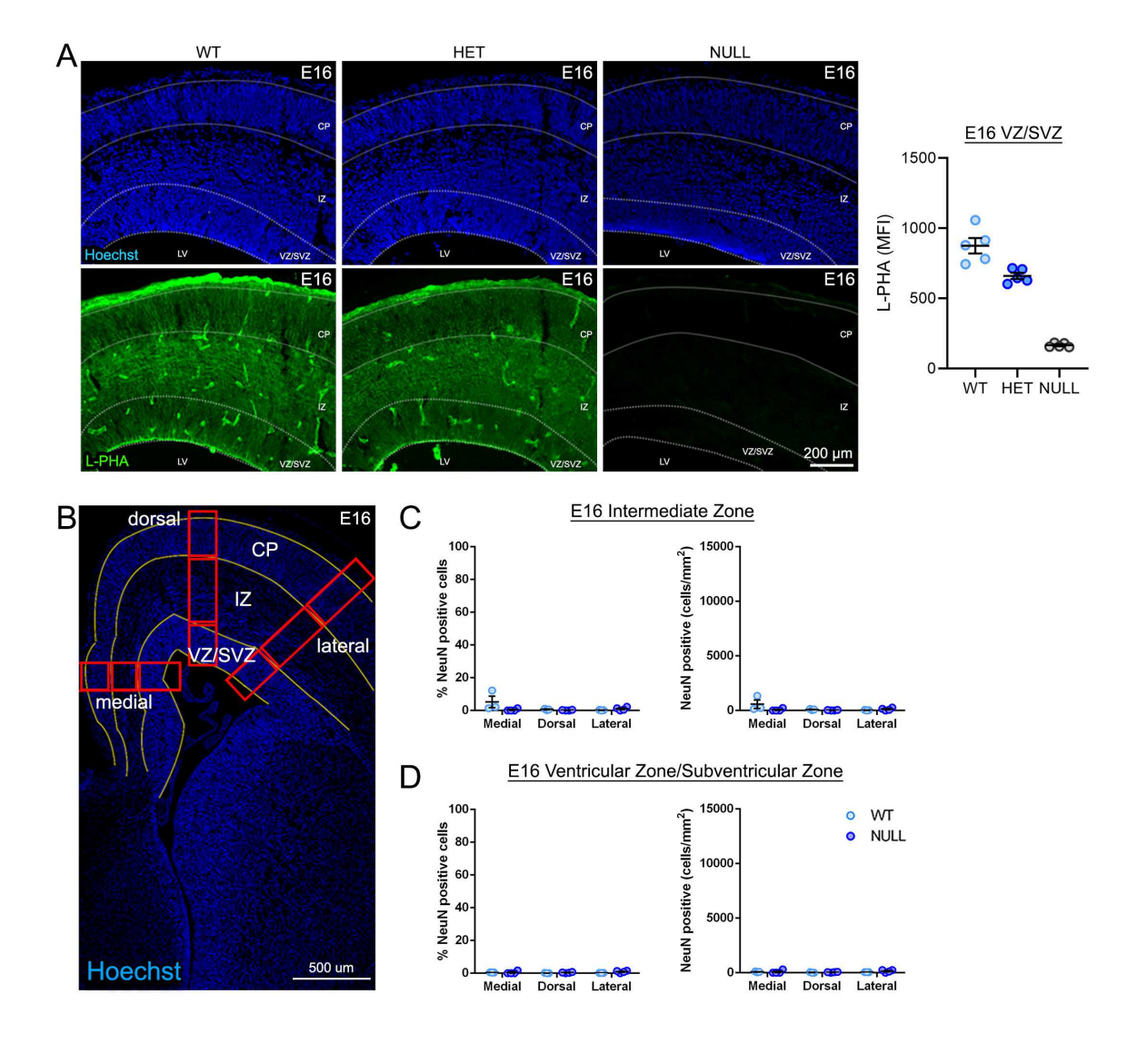


Figure S3. *Mgat5* null brains have reduced L-PHA binding and no difference in NeuN-positive cells in the intermediate zone or ventricular/subventricular zone compared to WT (related to Figure 3).

- (A) Coronal sections of E16 brain cerebral cortices were labeled with L-PHA, a lectin that binds β1-6 branched N-glycans generated by MGAT5. Compared to WT, L-PHA signal intensity is somewhat reduced in the Mgat5 heterozygous knockout brain and abolished in the Mgat5 homozygous null brain. All nuclei were stained with Hoechst and the ventricle is toward the bottom of the images. N=1 mouse per genotype, 5 fields analyzed each genotype.
 (B) Regions for quantitation are schematized on a WT E16 coronal section of dorsal forebrain stained with Hoechst. Yellow lines indicate the boundaries of the cortical plate (CP),
- intermediate zone (IZ), and ventricular zone/subventricular zone (VZ/SVZ). Red boxes indicate representative medial, dorsal, and lateral regions used for quantitation. (C) NeuN immunostaining was quantified as either the percentage of positive cells or the number of positive cells per area (cells/ mm²) in the E16 intermediate zone (IZ). Very few NeuN
- positive cells were present in the IZ, and there was no difference between WT and null brains. (D) There were very few NeuN positive cells in the E16 VZ/SVZ and there was no significant difference across genotype in the percentage or number of NeuN positive cells in this region.

All nuclei were stained with Hoechst, the lateral ventricle is toward the bottom of the images, and analyses used unpaired two-tailed Student's t-test WT vs. null, N=3-4 mice per genotype. Lines and error bars in dot plots show mean with SEM, respectively. (CP: cortical plate, IZ: intermediate zone, VZ/SVZ: ventricular/subventricular zone, LV: lateral ventricle).

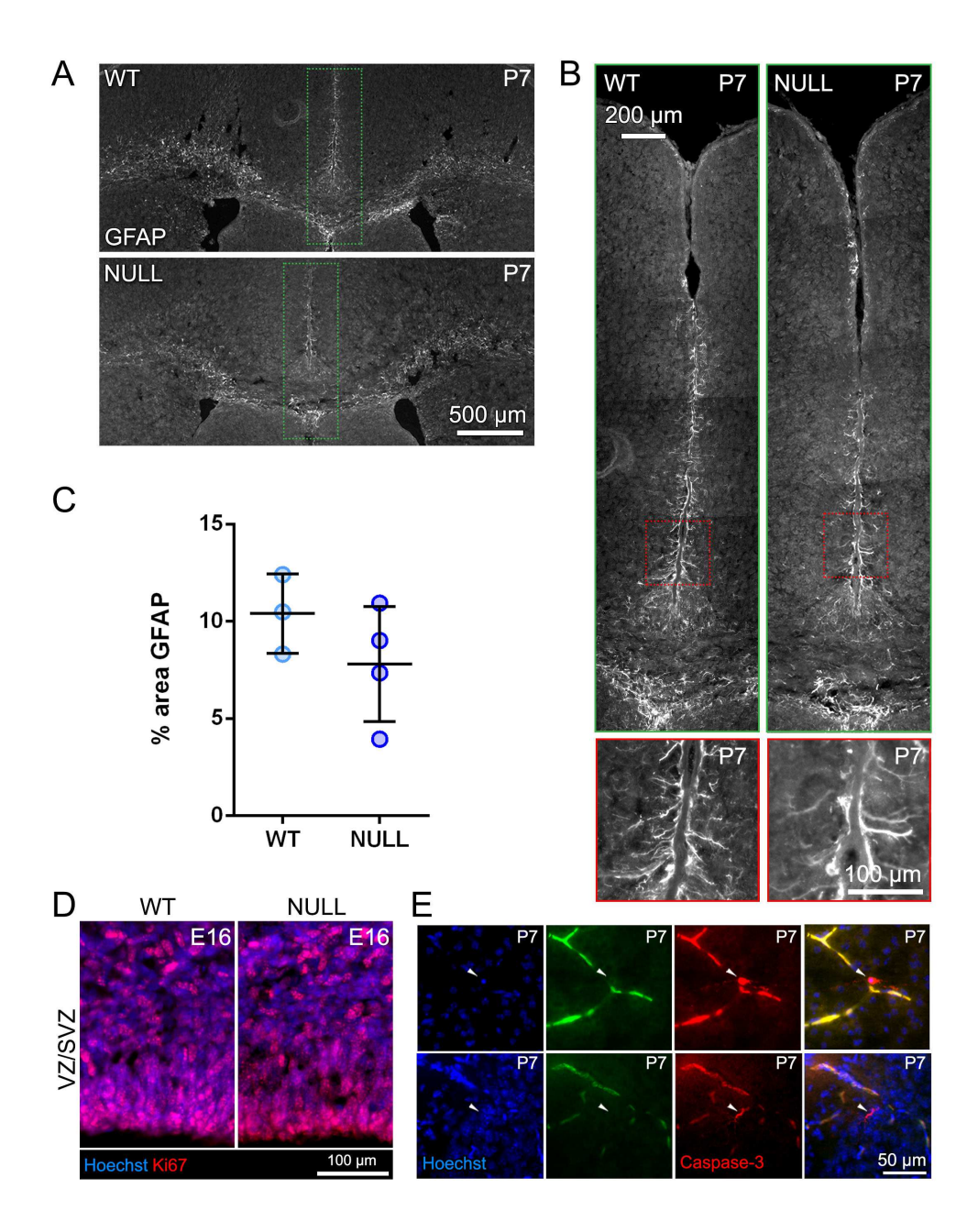


Figure S4. GFAP, Ki67 and Caspase-3 labeling do not differ between WT and *Mgat5* null brains (related to Figure 3).

- (A) Coronal sections from P7 WT and *Mgat5* null brains were immunostained to detect GFAP. At P7, GFAP labeling was primarily restricted to white matter tracts and cortical areas along the pial surface at the midline. Dashed green boxes indicate areas magnified in B.
- (B) Magnified images of the midline region show further detail of GFAP-positive cells in WT and *Mgat5* null brains. Dashed red boxes indicate areas further magnified in the lower panel red-bordered boxes.
- (C) GFAP expression was quantified near the pial surface of the cingulate cortex along the midline as the percent GFAP-positive area, such as shown by the dotted red boxes indicated in B. There was a non-significant decrease in GFAP-positive area in Mgat5 null cortex compared to WT.

- (D) Ki67 staining to mark proliferating cells in the E16 VZ/SVZ of the lateral cortical region show no difference between WT and null brains. Lateral ventricle is toward the bottom of each image. Quantitation is shown in Figure 3F.
- (E) P7 brain cortices were immunostained to detect cleaved Caspase-3 (red) to assess apoptotic cell death. Representative images from WT brain show Caspase-3 positive cells in deep (top panels) and upper (bottom panels) layers of the neocortex. Blood vessels display non-specific autofluorescence shown in green. White arrowheads denote locations of positively stained cells. Quantitation from WT and null brain is shown in Figure 3G.

Analyses used unpaired two-tailed Student's t-test WT vs. null, N=3-4 mice per genotype. Lines and error bars in dot plots show mean with SEM, respectively.

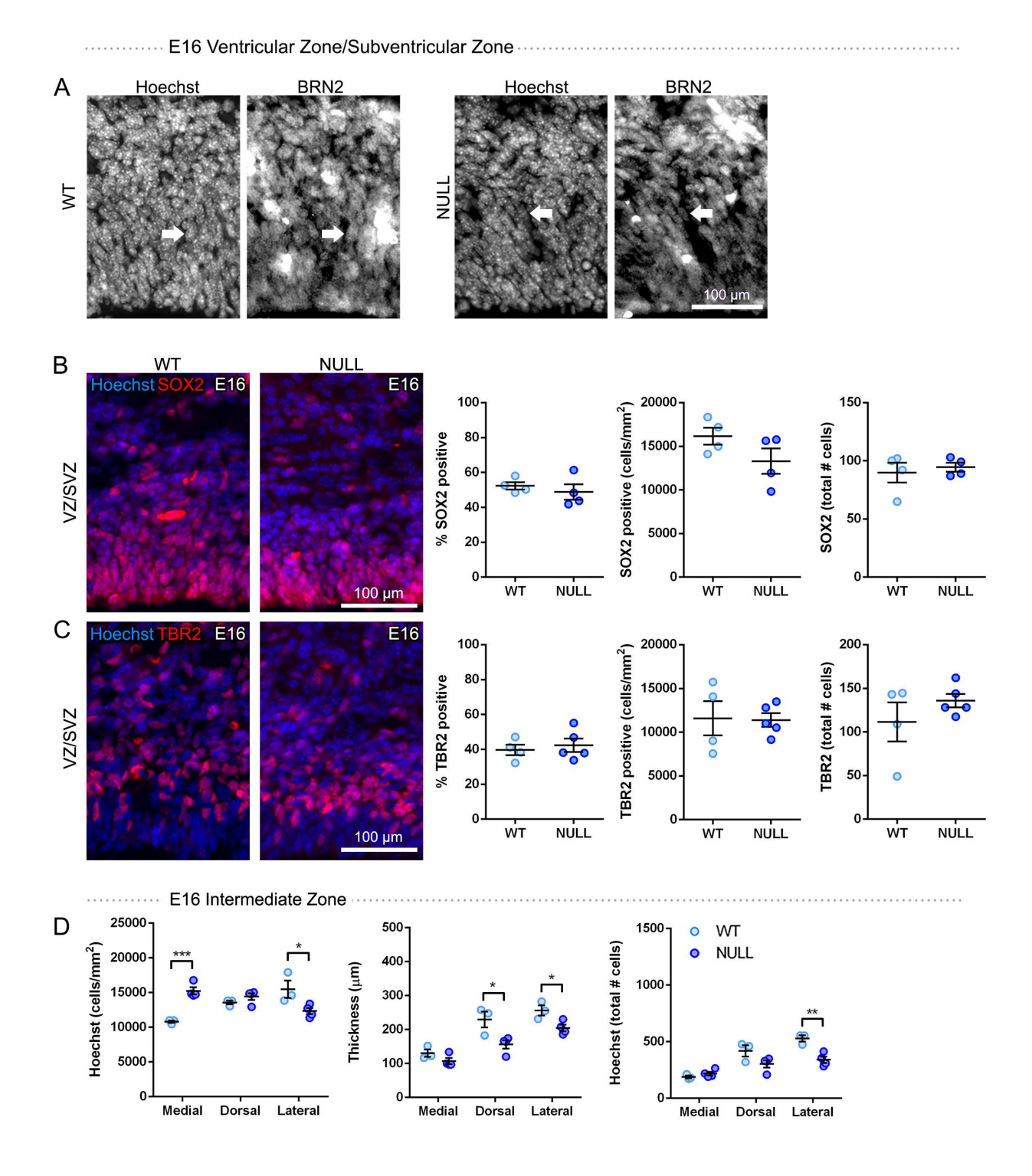


Figure S5. BRN2 immunostaining labels nuclei, MGAT5 deficiency does not alter SOX2 and TBR2 positive cells in the VZ/SVZ but does reduce cell number and thickness of the intermediate zone (related to Figure 5).

(A) BRN2 immunostaining detects upper layer neuron progenitor cell nuclei in the E16 dorsal VZ/SVZ of WT and null brains. All nuclei were stained with Hoechst, the ventricle is toward the bottom of the images, and arrows provide reference for nuclear staining. Images are grayscale versions of those in Figure 5B.

- (B) Immunostaining to detect SOX2 in E16 WT and *Mgat5* null VZ/SVZ showed a slight but nonsignificant decrease in SOX2-positive cells per mm² and no difference in the percentage or total number of SOX2-positive cells between the samples.
- (C) Analysis of TBR2, an intermediate progenitor marker, indicated no difference in TBR2-positive cells between WT and *Mgat5* null VZ/SVZ regions.
- (D) The number of Hoechst-stained cells per mm² was significantly decreased in the Mgat5 null lateral intermediate zone (IZ) compared to WT at E16 (p=0.0442). In contrast, Mgat5 null medial IZ shows higher cell density than WT (p=0.0009). The thickness of the Mgat5 null IZ was significantly reduced in dorsal (p=0.0300) and lateral (p=0.0286) regions compared to WT. The total number of Hoechst-stained cells was significantly reduced in the Mgat5 null lateral IZ compared to WT (p=0.0058).

All nuclei were stained with Hoechst, the ventricle is toward the bottom of the images, and analyses used unpaired two-tailed Student's t-test WT vs. null, N=3-5 mice per genotype. Lines and error bars in dot plots show mean with SEM, respectively, *p<0.05, **p<0.01, ***p<0.001.

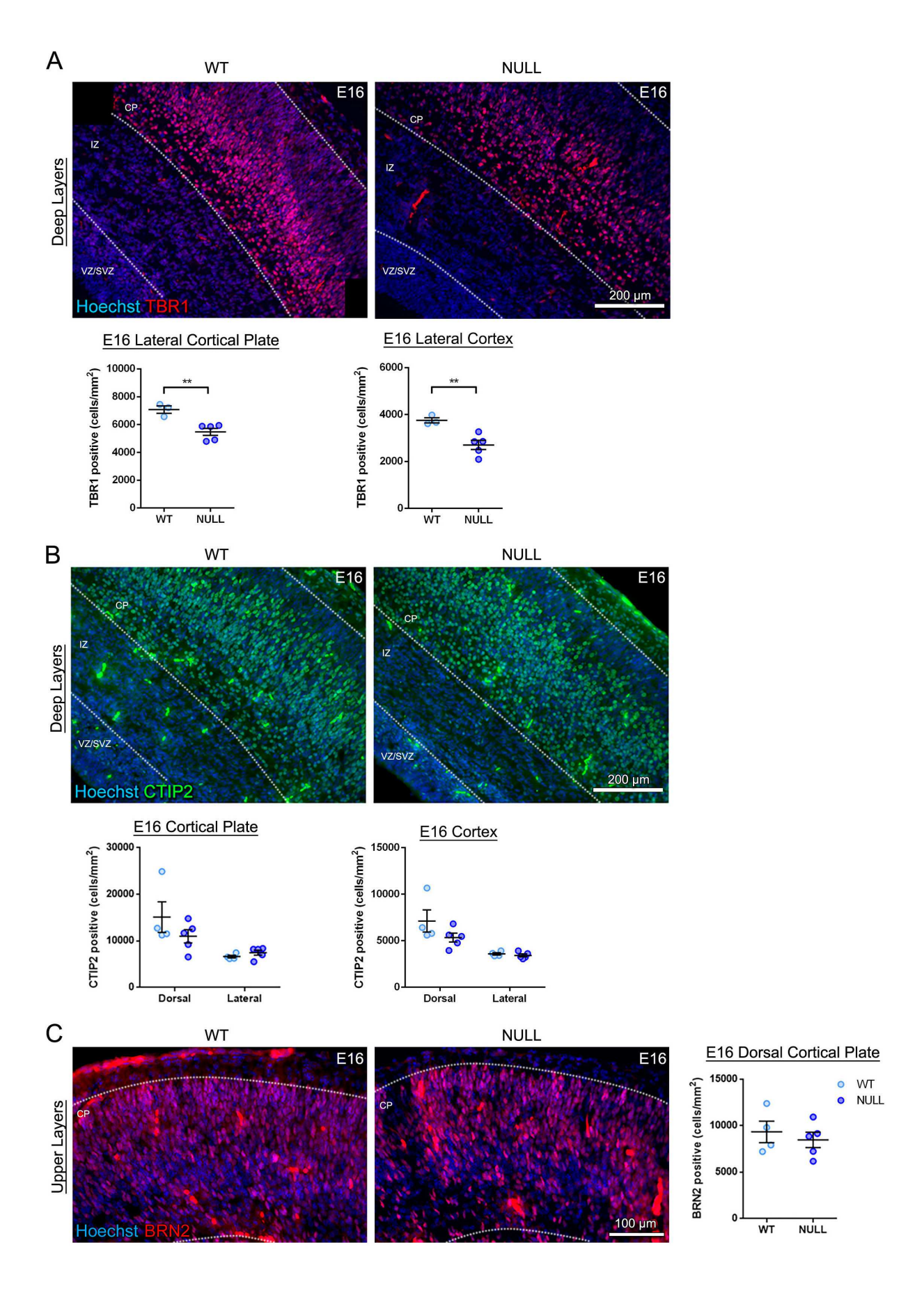


Figure S6. TBR1-positive deep layer neurons are reduced in *Mgat5* null brains at E16 while CTIP2-positive layer 5 and BRN2-positive upper layer neurons do not differ (related to Figure 6).

- (A) Coronal sections of E16 brain were immunostained to detect deep layer neuron marker TBR1 (layer 6) in the lateral CP and cortex. The ventricle is toward the bottom left corner of the image. TBR1-positive neurons were significantly reduced in the *Mgat5* null lateral CP (p=0.0065) and cortex (p=0.0091) compared to WT. Images and CP data are as shown in Figure 6A and included for comparison.
- (B) Coronal sections of E16 brain were immunostained to detect deep layer neuron marker CTIP2 (layers 5/6) in the dorsal and lateral CP and cortex (combined CP, IZ, and VZ/SVZ). The ventricle is toward the bottom left corner of the image. There was no significant difference in CTIP2 in the dorsal or lateral CP or cortex between WT and *Mgat5* null.
- (C) Coronal sections of E16 brain were immunostained to detect upper layer neuron marker BRN2 (layers 2/3) in the dorsal cortical plate (CP). The ventricle is toward the bottom of the image. There was no significant difference in BRN2 between E16 WT and null brains. All nuclei were stained with Hoechst and analyses used unpaired two-tailed Student's t-test WT vs. null, N=3-5 mice per genotype. Lines and error bars in dot plots show mean with SEM, respectively, **p<0.01.

Supplemental Experimental Procedures

Animals and genotyping

All animal procedures were in accordance with protocols approved by the University of California, Irvine Institutional Animal Care and Use Committee and adhered to National Institutes of Health Guidelines for the Care and Use of Laboratory Animals. Mice were CD1 (Charles River) or *Mgat5* C57BL/6 knockouts containing a *lacZ* gene insert in the *Mgat5* coding region that inactivates the enzyme (provided by Dr. Michael Demetriou) (Granovsky et al. 2000, Lee et al. 2007). Heterozygous *Mgat5* knockout mice (*Mgat5* +/-) were bred to generate pups with wild type (*Mgat5* +/+), heterozygous (*Mgat5* +/-), or homozygous (*Mgat5*-/-) null alleles. Mice pups were genotyped to detect a *lacZ* gene insertion in *Mgat5* null alleles that disrupts the coding portion of exon 1 (Granovsky et al. 2000). Genotyping was done in house using standard PCR with the following primers for *Mgat5* (forward: 5' - GCC AAG GGA ATG GTA CAT TGC – 3'; reverse: 5' - GGA GTC GAC ACT CAG GAA TG – 3') and LacZ (forward: 5' - CCC ATC TAC ACC AAC GTA ACC – 3'; reverse: 5' - CCT TCT AGT CCT ATA CAC CGC – 3') or by Transnetyx. The wild type *Mgat5* allele is detected as an ~400 base pair amplicon while the *Mgat5* null allele generates an ~300 base pair product.

Cell culture and differentiation

NSPCs were collected from dorsal forebrain cortical tissue that was dissected from the cerebral cortices of embryonic day 12.5 (E12), 16.5 (E16), or 18.5 (E18) mice and placed in dissection buffer: PBS, 0.6% glucose, 50 U/mL Pen/Strep (Yale et al. 2018). Cortical tissue was dissociated using 0.05% Trypsin-EDTA at 37° C for 10 min. Afterward, trypsin was inhibited using soybean trypsin inhibitor (Life Technologies) and dissociated cells were re-suspended in proliferation medium containing DMEM, 1x B27, 1x N2, 1 mM sodium pyruvate, 2 mM Lglutamine, 1 mM N-acetylcysteine, 20 ng/mL EGF, 10 ng/mL bFGF, and 2 µg/mL heparin. Cells were seeded at 150,000 cells/mL into non-tissue culture treated plastic plates and grown as non-adherent spheres. NSPC cultures were passaged approximately every 3 days using enzyme-free NeuroCult Chemical Dissociation Kit (Mouse) (StemCell Technologies). All NSPC cultures were passaged at least once after dissection prior to experimental use. For CD1 mice, cortical tissue from multiple embryos within the same litter was pooled, and a subsequent culture from a single litter was considered a biological repeat. For Mgat5 mutant mice, NSPCs derived from each embryo were kept separate and genotyped. Each NSPC culture from a single embryo was maintained separately and considered a biological repeat. Comparisons across genotype utilized at least 3 embryos per genotype from separate litters (not littermates).

NSPCs were plated as adherent cultures for differentiation (Yale et al. 2018). HCl-washed German glass coverslips (Assistant/Carolina Biological Supply, Burlington, NC) were pretreated with poly-D-lysine (40 μ g/mL in milliQ H₂O) for 5 minutes then coated with laminin (20 μ g/mL in EMEM) at 37° C for 24 hours prior to cell adhesion. Whole neurospheres were seeded onto the laminin-coated coverslips in proliferation medium. After 24 hours, proliferation medium was removed and replaced with differentiation medium (same components as proliferation medium but excluding EGF, bFGF, and heparin) to induce differentiation. NSPCs were differentiated into neurons and astrocytes in these conditions for 3 days and oligodendrocytes for 7 days. For 7 day differentiated samples, differentiation medium was replaced after 3 days.

Cell treatment

A stock solution of 800 mM N-acetylglucosamine (GlcNAc,Thermo Fisher Scientific, 10-792) was prepared in proliferation medium and diluted to a final concentration of 80 mM in proliferation medium for treatment (Yale et al. 2018). NSPCs were treated for 3 days, with fresh GlcNAc added every 24 hours since GlcNAc breaks down over time in aqueous solutions. GlcNAc was not added during differentiation.

Kifunensine was used to inhibit mannosidase I. A 1 mg/ml (4.3 mM) stock solution of Kifunensine (Sigma-Aldrich, K1140) in H_2O was diluted in proliferation medium to generate concentrations of 0.001, 0.01, 0.02, 0.05, 0.1, 0.2, 0.3, 0.5, 1, 2, 5, 10 μ M. NSPCs were treated for 1 day (0.5 μ M concentration, E12 NSPCs) or 4 days (all concentrations for E12 NSPCs, 0.5 μ M concentration for E16 and E18 NSPCs) in proliferation medium and Kifunensine was not added during differentiation.

E12 and E16 NSPCs were treated with either 1 μ M deoxymannojirimycin (DMJ, EMD Millipore, 260575) to inhibit mannosidase I or 500 nM swainsonine (SW, Sigma Aldrich, S8195) to block mannosidase II during growth in proliferation medium for 3 days and as the cells were differentiating for 3-5 days (Nourse et al. 2014).

Flow cytometry to assess lectin binding and cell viability

For flow cytometry, live E12 mouse NSPCs were dissociated using the NeuroCult dissociation kit and re-suspended in 1x PBS with 5% BSA. Cells were incubated with various fluorescein-conjugated lectins for 1 hour on ice in the dark. See Table S2 for lectins and concentrations. All cells were counter-stained with 50 μ g/ml propidium iodide (Thermo Fisher, P3566) for 5 minutes prior to flow cytometry to exclude dead cells from analysis. Cell viability was assessed using the LIVE/DEAD Viability/Cytotoxicity Kit (for mammalian cells) (Thermo Fisher Scientific, L3224). Briefly, E12 mouse NSPCs dissociated using the NeuroCult dissociation kit were re-suspended in 1 mL proliferation medium containing 100 nM calcein-AM to label live cells and 8 μ M ethidium homodimer-1 to label dead cells. The cell suspension was incubated for 15-20 min at room temperature, protected from the light. Cell samples were analyzed on a BD LSR II flow cytometer, and the data was collected using BD FACSDIVA software. All data analysis was performed using FlowJo v10.1.

Immunocytochemistry and quantitation of cultured cells

Cell culture samples were fixed with 4% paraformaldehyde (4% paraformaldehyde, 5 mM MgCl₂, 10 mM EGTA, 4% sucrose in PBS) for 10 min, and cell membranes were permeabilized with 0.3% Triton X-100 in PBS for 5 min. Cells immunostained to detect O4 were not permeabilized with Triton X-100 since O4 is a cell surface antigen. Non-specific binding was blocked using 5% BSA in PBS for 1 hour then incubated with the primary antibody for approximately 18 hours at 4° C and the secondary antibody for 2 hours at room temperature in the dark. Primary and secondary antibodies were diluted in 1% BSA in 1x PBS. All cells were counterstained with Hoechst 33342 nuclear dye (Life Technologies, H1399) and coverslips were mounted onto glass slides using ProLong Diamond Antifade Mountant medium (Thermo Fisher Scientific, P36970). Cells were visualized using a Nikon Eclipse Ti-E fluorescence microscope at 20x magnification, and all images were acquired using NIS Elements AR 4.51 image capturing and analysis software. See Table S2 for antibodies and concentrations.

For analysis, at least 3 independent sets of NSPCs derived from 3 different litters were analyzed using manual counting software built into ImageJ. Positively labeled cells were counted as a percentage of all Hoechst-stained cells in 5 randomly selected fields. The percentage of cells that differentiated into double-positive MAP2/TUJ1 neurons with neurite lengths of at least 3 times the length of the soma was calculated from more than 1000 cells counted per experimental group in each of the 3 independent experiments, so over 3000 cells per group. The percentages of GFAP-positive astrocytes were calculated from randomly selected fields of cells adjacent to the sphere attachment site but not from the dense cells within the sphere since cell density and cell death affect astrocyte GFAP reactivity. Cells expressing GFAP in a filamentous cytoskeletal pattern were counted as astrocytes and 3000 or more cells per experimental group were analyzed. Cells expressing O4 on the cell surface and extending ramified processes at least 2 times the length of the cell body were counted as oligodendrocytes.

Proliferation assays of cultured cells

E12 mouse NSPCs were plated as neurospheres on laminin-coated coverslips in proliferation medium for 24 hours. After fixation, cells were immunostained to detect Ki67 as a marker of actively cycling cells or phospho-histone H3 to detect cells undergoing mitosis. All cells were counterstained with Hoechst 33342 nuclear dye. See Table S2 for antibodies and concentrations. To visualize cells in S-phase, adherent E12 mouse NSPCs were treated with 10 µM 5-ethynyl-2′-deoxyuridine (EdU, Click-iT EdU Alexa Fluor 555 Imaging Kit, Thermo Fisher Scientific, C10338) in proliferation medium at 37° C for 4 hours. Cells were fixed and permeabilized as described above then incubated with the EdU Click-iT reaction cocktail for 30 min at room temperature in the dark and counterstained with Hoechst 33342 nuclear dye. Quantitation of positively-labeled cells was as described above.

Flow cytometry cell cycle analysis was performed by dissociating NSPCs and fixing suspended cells using cold 70% ethanol for 30 min at 4° C. Fixed cells were incubated with DNAse-free ribonuclease (Thermo Fisher, EN0531) for 45 min at 37° C to remove RNA. Cells were then incubated in 2.5 μ g/mL propidium iodide for 30 min on ice and each sample volume was increased to 500 μ L using PBS. All cells were analyzed on a BD LSR II flow cytometer, and the data was collected using the BD FACSDIVA software. Cell cycle data analysis was performed using the built-in program in FlowJo v10.1.

RNA sequencing and analysis

RNA sequencing and analysis for mNSPCs was as previously described (Yale et al. 2018). RNA was isolated from suspended E12 CD1 mouse NSPC cultures from three separate litters using the Bio-Rad RNA Isolation Kit (Genicity, Irvine, CA, USA; G00065). Genomic DNA contamination of all RNA samples was assessed by using qRT-PCR for mouse 18S and *Gapdh* with and without reverse transcriptase and found to be insignificant. cDNA for qRT-PCR was synthesized using M-MLV reverse transcriptase (Promega). Total RNA was further monitored for quality control using the Agilent Bioanalyzer Nano RNA chip and Nanodrop absorbance ratios for 260/280 nm and 260/230 nm.

RNA library preparation and sequencing was performed at the UCI Genomics Core as previously described (Arulmoli et al. 2016). Library construction was performed according to the Illumina TruSeq mRNA stranded protocol. The input quantity for total RNA was 250 ng and mRNA was enriched using oligo dT magnetic beads. The enriched mRNA was chemically fragmented for five minutes. First strand synthesis used random primers and reverse transcriptase to make cDNA. After second strand synthesis the double-stranded cDNA was cleaned using AMPure XP beads and the cDNA was end repaired and the 3' ends were adenylated. Illumina barcoded adapters were ligated on the ends and the adapter ligated fragments were enriched by nine cycles of PCR. The resulting libraries were validated by qPCR and sized by Agilent Bioanalyzer DNA high sensitivity chip. The concentrations for the libraries were normalized and the libraries were multiplexed together. The concentration for clustering on the flowcell was 12.5 pM. The multiplexed libraries were sequenced on one lane using single read 100 cycles chemistry for the HiSeq 2500. The version of HiSeq control software was HCS 2.2.58 with real time analysis software, RTA 1.18.64.

For sequence mapping and bioinformatic analysis, RNA-Seq data was processed as described previously (Lissner et al. 2015). All bioinformatics analyses were conducted using the Galaxy platform (Goecks et al. 2010). Reads were aligned to the mouse NCBI37/mm9 reference genome with the TopHat program (Trapnell et al. 2010) using most default parameters. Alignments were restricted to uniquely mapping reads with two possible mismatches permitted. RPKM (reads per kilobase pair per million mapped reads) were calculated as described (Mortazavi et al. 2008) for mm9 RefSeq genes using the SeqMonk program (http://www.bioinformatics.babraham.ac.uk/projects/seqmonk/). mRNA RPKMs were derived by counting exonic reads and dividing by mRNA length.

Analysis of glycosylation enzyme expression was performed using qRT-PCR. RNA was isolated from E12 *Mgat5* WT and null mouse NSPCs using Aurum Total RNA Mini Kit (Bio-Rad Laboratories) and qRT-PCR was performed using PowerUp™ SYBR® Green Master Mix (Thermo Fisher Scientific). Short oligonucleotide DNA primers were customized through NCBI's Primer-BLAST or used sequences from the MGH PrimerBank (Mgat1 ID: 31981620a1 and Mgat 4b ID: 253683469c3) (Spandidos et al. 2010) and primers were ordered from IDT (Table S1). Primers were used at an annealing temperature of 65° C and all qRT-PCR experiments were performed using Applied Biosystems QuantStudio 6 or 7 RT-PCR systems. Samples lacking either reverse transcriptase or cDNA were used for quality control. Data was analyzed by the comparative cycle (C₁) method (Cheng et al. 2006) using the housekeeping gene cyclophilin A (CypA, PPIA) for normalization. Gene expression was further normalized to RNA isolated from whole E16 cerebral cortex to obtain relative expression values.

Table S1: DNA primers for qRT-PCR.

Gene	Forward Primer (5' 3')	Reverse Primer (5' 3')	Expected length (bp)
Mgat1*	TTGTGCTTTGGGGTGCTATCA	CCACAGTGGGAACTCTCCA	249
Mgat2	GTGGATTTCTGCCCGGTTCT	AGGAGTCAGGGTATTCGGCA	157
Mgat3	CCAGCGGACGATGGGATGAA	GGTGTCCGCAATAGGTCGGG	233
Mgat4a	TTTGTTCCACAGCGGCAATC	GGCCCAAACAGCTGAGTTCT	244
Mgat4b*	GGACCAAACAGAACCTCGATT	CAACTGCGAGAACTCCAGGAT	176
Mgat5	TAGGTCATCAGAATGGAAGCCCA	GCCCAGCTTCTGAGAGGACA	195
Fut8	TCTATGGGGAGGAAGCATGTAG	CAGTCCATGCCCGCATTTTC	262
St6gal1	GGCACCTTTAACCTTGAGCC	GGACGCTTGGTCTCCGTTAT	124
СурА	GAGCTGTTTGCAGACAAAGTTC	CCCTGGCACATGAATCCTGG	213

^{*}MGH PrimerBank

Preparation of brain sections

Whole brains were dissected from Mgat5 WT, heterozygous, and null animals at E16 and P7. Brains were drop fixed in 4% paraformaldehyde for approximately 18 hours at 4° C then transferred to 30% sucrose in 1x PBS. Brains were incubated in the sucrose solution until the tissue was no longer floating. Sucrose-permeated brains were quickly frozen in Optimal Cutting Temperature (OCT) compound (Tissue-Tek, VWR 25608-930) and stored at -80° C prior to sectioning. All brains were cut on a Leica research cryostat (Leica CM3050 S) into 12 μ m thick coronal sections mounted on SuperFrost glass slides. OCT was dissolved by submerging slides in 1x PBS for 5 min.

Lectin staining of brain sections

Brain sections were washed with PBS and blocked for 20 min at room temperature with 3% BSA in PBS with 0.1% Triton X-100. Sections were incubated with FITC-conjugated lectin Phaseolus vulgaris leukagglutinin (L-PHA) at 20 µg/mL (Vector Labs, FL-1111) in blocking solution for 1 hour at room temperature in a humidified chamber. Sections were counterstained with Hoechst 33342 nuclear dye (Thermo Fisher Scientific, 62249) and mounted with ProLong Gold Antifade Mountant medium (Thermo Fisher Scientific, P36934).

Immunohistochemistry and quantitation of brain sections

Brain sections were immunostained to detect NeuN, TuJ1, BRN2, CTIP2, TBR1, Ki67, SOX2, TBR2, cleaved Caspase-3, and GFAP. See Table S2 for antibodies and concentrations. For staining with antibodies for BRN2, CTIP2, TBR1, Ki67, TBR2, and cleaved Caspase-3, sections were subjected to antigen retrieval in a sodium citrate buffer (10 mM sodium citrate, 0.05% Tween 20, pH 6.0) for 1 hour in a pressure cooker prior to blocking. Sections were blocked for 20 min in 1x PBS with 0.1% Triton X-100 (PBST) and 5% donkey serum (DS). Primary antibodies were diluted in PBST with 5% DS and the sections were incubated with the primary antibody overnight at 4° C in a humidified chamber. After washing, sections were incubated with secondary antibody diluted in PBST with 5% DS for 1 hour at room temperature. All sections were counter-stained with Hoechst 33342 and mounted with ProLong Gold or Diamond Antifade Mountant medium. Sections were visualized using a Nikon Eclipse Ti-E fluorescence microscope, and all images were acquired using NIS Elements AR 4.51 image capturing and analysis software.

Overlapping gradients control differentiation temporally and spatially in the developing mouse brain. Morphogen and growth factor gradients in the developing telencephalon are critical for the formation of specific cortical regions at precise locations during development (Sansom and Livesey 2009). The cell composition and developmental "stage" of the cortex vary significantly across location due to these gradients, which extend in both rostral-caudal and medial-lateral directions. Thus, when comparing developing cerebral cortex sections across animals it is important to match the location of each section for analysis. In order to match locations along the brain rostral-caudal axis of the E16 brain, images were taken of coronal sections ranging from the anterior horn of the lateral ventricle when the medial septal nucleus is visible to more posterior regions where the midline begins to enlarge and fold to form the hippocampus. Layers of the E16 brain (CP, IZ, VZ/SVZ) were defined by patterns of Hoechst-stained nuclei. To match locations along the medial-lateral axis we defined medial, dorsal, and lateral regions for analysis, which were located medially (across the ventricle from the ganglionic eminence fold), dorsally (from the most dorsal aspect), and laterally (adjacent to the ganglionic eminence fold) in each section. Boxes for quantitation were drawn to encompass the entire layer within the region (for example, lateral CP, IZ and VZ/SVZ) and the summation of CP, IZ, and VZ/SVZ boxes corresponded to the total cortex.

For P7 brain, images were taken of coronal sections from lateral regions of the somatosensory cortex of the anterior forebrain starting where the genu of the corpus callosum crosses both hemispheres and continuing caudally until the anterior commissure visibly forms an interhemispheric junction. Quantitation of cleaved Caspase 3 in the P7 brain focused on the cortical plate (defined as the region above the white matter tracts). Boxes were drawn from the edge of the white matter tracts to the pial surface to define the region of analysis for the cortical plate. Images of P7 brain sections to assess GFAP staining were taken of coronal sections from lateral regions of the somatosensory cortex of the anterior forebrain starting where the genu of the corpus callosum crosses both hemispheres and continuing caudally until the anterior commissure visibly forms an interhemispheric junction to provide matched samples across genotype. Quantitation of GFAP at P7 focused on staining in the medial regions of the cortex since GFAP labeling was primarily restricted to cortical areas along the pial surface at the midline and white matter tracts at this stage. A box (300x300 µm) was drawn along the medial pial surface and the percentage of the area with positive GFAP staining was quantified for each brain section. For analysis of layers 2/3, 4, and 5/6, nuclei patterns were used to discern the layers and 3 boxes (200x100 µm) were drawn within the layer. This approach made it possible to focus analysis in the middle of each layer to avoid layer boundaries.

For both E16 and P7, data were analyzed from 3 or more brains per genotype. Antibody and Hoechst staining were used to quantify the following: the percentage of positively stained cells

(number positively stained/total number Hoechst stained cells), cells/mm² (number positively stained per unit area), total cell number (total number positively stained in the region). The thickness of regions or layers was measured using images of Hoechst stained sections to define architectural boundaries and ImageJ to determine distance between boundaries.

Graphs and statistical analysis

Graphing and statistical analysis used Prism v.6 software (GraphPad). Lines in dot plots show mean and the bars show standard error of the mean. For box plots, the box extends from the 25th to 75th percentiles, the line in the middle of the box is the median, and the boxes have Tukey whiskers. Comparison of two samples utilized two-tailed unpaired Student's t-tests. Datasets containing more than two samples were analyzed by one-way ANOVA with Tukey's post hoc correction for multiple samples.

Table S2: Antibody and lectin reagents and concentrations.

Item	Vendor	Catalogue #	Antibody dilution or lectin final concentration
Anti-BRN2 (B-2), mouse IgG	Santa Cruz Biotechnology	SC-393324	IHC: 1:1000
Anti-Caspase-3, rabbit IgG	Cell Signaling Technologies	9661S	IHC: 1:1000
Anti-CTIP2 (25B6), rat IgG	Abcam	Ab18465	IHC: 1:1000
Anti-GFAP, rabbit IgG	Sigma	G9269	ICC: 1:200 IHC: 1:200
Anti-Ki67, rabbit IgG	Leica Biosystems	KI67P-CE	ICC: 1:200 IHC: 1:500
Anti-MAP2, mouse IgG	Sigma	M9942	ICC: 1:200
Anti-NeuN, rabbit IgG	EMD Millipore	ABN78	IHC: 1:100
Anti-O4, mouse IgM	R&D Systems	MAB1326	ICC: 1:100
Anti-Phospho-histone H3 (Ser10) (6G3), mouse IgG	Cell Signaling Technology	9706S	ICC: 1:200
Anti-SOX2, goat IgG	Santa Cruz Biotechnology	SC-17320	IHC: 1:200
Anti-TBR1, rabbit IgG	Abcam	Ab31940	IHC: 1:500
Anti-TBR2, rabbit IgG	Abcam	Ab23345	IHC: 1:500
TuJ1, anti-class III β tubulin, rabbit IgG	Sigma	T2200	ICC: 1:100 IHC: 1:200
Alexa Fluor 594 donkey anti- goat IgG	Jackson ImmunoResearch	705-585-147	IHC: 1:200
Alexa Fluor 488 donkey anti- mouse IgG	Jackson ImmunoResearch	715-545-151	ICC: 1:200 IHC: 1:200
			11.10. 1.200

Alexa Fluor 555 goat anti- mouse IgM	Invitrogen	A21426	ICC: 1:200
Alexa Fluor 594 donkey anti- rabbit IgG	Jackson ImmunoResearch	711-585-152	ICC: 1:200 IHC: 1:200
Alexa Fluor 594 donkey anti- rat IgG	Jackson ImmunoResearch	712-585-153	IHC: 1:500
Canavalia ensiformis concanavalin A (ConA), Fluorescein labeled	Vector Labs	FL-1001	Flow: 20 µg/ml
Datura stramonium lectin (DSL), Fluorescein labeled	Vector Labs	FL-1181	Flow: 20 µg/ml
Lycopersicon esculentum agglutinin (LEA, LEL), Fluorescein labeled	Vector Labs	FL-1171	Flow: 50 µg/ml
Lens culinaris agglutinin (LCA), Fluorescein labeled	Vector Labs	FL-1041	Flow: 20 µg/ml
Phaseolus vulgaris erythroagglutinin (E-PHA), Fluorescein labeled	Vector Labs	FL-1121	Flow: 20 μg/ml
Phaseus vulgaris leucoagglutinin (L-PHA), Fluorescein labeled	Vector Labs	FL-1111	Flow: 20 μg/ml IHC: 1:100
Sambucus nigra agglutinin (SNA), Fluorescein labeled	Vector Labs	FL-1301	Flow: 40 μ g/ml

Supplemental References

- Arulmoli, J., H. J. Wright, D. T. Phan, U. Sheth, R. A. Que, G. A. Botten, M. Keating, E. L. Botvinick, M. M. Pathak, T. I. Zarembinski, D. S. Yanni, O. V. Razorenova, C. C. Hughes and L. A. Flanagan (2016). "Combination scaffolds of salmon fibrin, hyaluronic acid, and laminin for human neural stem cell and vascular tissue engineering." <u>Acta Biomater</u> **43**: 122-138.
- Cheng, X., C. M. Hsu, D. S. Currle, J. S. Hu, A. J. Barkovich and E. S. Monuki (2006). "Central roles of the roof plate in telencephalic development and holoprosencephaly." <u>J Neurosci</u> **26**(29): 7640-7649.
- Goecks, J., A. Nekrutenko, J. Taylor and T. Galaxy (2010). "Galaxy: a comprehensive approach for supporting accessible, reproducible, and transparent computational research in the life sciences." Genome Biol **11**(8): R86.
- Granovsky, M., J. Fata, J. Pawling, W. J. Muller, R. Khokha and J. W. Dennis (2000). "Suppression of tumor growth and metastasis in Mgat5-deficient mice." <u>Nat Med</u> **6**(3): 306-312.
- Lee, S. U., A. Grigorian, J. Pawling, I. J. Chen, G. Gao, T. Mozaffar, C. McKerlie and M. Demetriou (2007). "N-glycan processing deficiency promotes spontaneous inflammatory demyelination and neurodegeneration." J Biol Chem **282**(46): 33725-33734.
- Lissner, M. M., B. J. Thomas, K. Wee, A. J. Tong, T. R. Kollmann and S. T. Smale (2015). "Age-Related Gene Expression Differences in Monocytes from Human Neonates, Young Adults, and Older Adults." <u>PLoS One</u> **10**(7): e0132061.
- Mortazavi, A., B. A. Williams, K. McCue, L. Schaeffer and B. Wold (2008). "Mapping and quantifying mammalian transcriptomes by RNA-Seq." <u>Nat Methods</u> **5**(7): 621-628.
- Nourse, J. L., J. L. Prieto, A. R. Dickson, J. Lu, M. M. Pathak, F. Tombola, M. Demetriou, A. P. Lee and L. A. Flanagan (2014). "Membrane biophysics define neuron and astrocyte progenitors in the neural lineage." <u>Stem Cells</u> **32**(3): 706-716.
- Sansom, S. N. and F. J. Livesey (2009). "Gradients in the brain: the control of the development of form and function in the cerebral cortex." <u>Cold Spring Harb Perspect Biol</u> **1**(2): a002519.
- Spandidos, A., X. Wang, H. Wang and B. Seed (2010). "PrimerBank: a resource of human and mouse PCR primer pairs for gene expression detection and quantification." <u>Nucleic Acids Res</u> **38**(Database issue): D792-799.
- Trapnell, C., B. A. Williams, G. Pertea, A. Mortazavi, G. Kwan, M. J. van Baren, S. L. Salzberg, B. J. Wold and L. Pachter (2010). "Transcript assembly and quantification by RNA-Seq reveals unannotated transcripts and isoform switching during cell differentiation." <u>Nat Biotechnol</u> **28**(5): 511-515.
- Yale, A. R., J. L. Nourse, K. R. Lee, S. N. Ahmed, J. Arulmoli, A. Y. L. Jiang, L. P. McDonnell, G. A. Botten, A. P. Lee, E. S. Monuki, M. Demetriou and L. A. Flanagan (2018). "Cell surface N-glycans influence electrophysiological properties and fate potential of neural stem cells." Stem Cell Reports 11(4): 869-882.